Thesis Title

Thesis Subtitle

Nathan Frederick Smith

A thesis presented in partial fulfillment of the degree of
Master's of Science

Department of Physics
McGill University, Montreal
Canada
??-??-2017

Dedication

Dedication here...

Acknowledgements

- Nik for a million things
- Quentin Stoyel for helping edit
- Matt Frick for editing help

Abstract

English abstract...

Abrégé

French abstract...

Contents

List of Figures

List of Tables

List of Symbols

$*$	Denotes an inner product (where appropriate) and integration over repeated variables.

Chapter 1

Introduction

The study of two binary alloys in materials physics is a pursuit of incredibly broad impact. Industries as distant as the large commerial materials such as steel and aluminium producers and burgeoning markets of nano-fabrication and optoelectronics are affected by research in binary alloys.

One suprising aspect of binary alloys is the rich diversity of properties and behaviours they display. Because material properties depend on the microstructural details of the material they have a strong path dependence. Grain boundaries, vacancies, dislocations and other microstructural are all intimitly tied to the manufactoring process of the alloy. This means that the study of solids can never be completely seperated from the study of solidification. As such the diversity of material properties and behaviours we see in binay alloys can be directly attributed to the diversity of processes for their construction.

Given the importance of these systems it is important to construct models that can explain diversity of behavior we see in them. At the moment models of solidification can be categorized by the length and time scales they accurately discribe. The the macroscopic length and time scales we have continuum methods of heat and mass transport and associated finite element methods of analysis. These methods are appropriate for studying large castings for example. On length scales $\mathcal{O}(10^{-3})m$ to $\mathcal{O}(10^{-6})$ we use *Phase Field* methods to study

phenomena such as dendritic growth and chemical segregation. On still finer length scales from $\mathcal{O}(10^{-9})$ to $\mathcal{O}(10^{-6})$ and on relatively long timescales we have the methods of *Phase Field Crystal* theory and dislocation dynamics. These methods are appropriate for studying nanoscopic changes that occur on diffusive timescales such as dislocation motion, creep, grain boundary motion and micro segregation. At a still finer scale and on very short time scales ($\mathcal{O}(10^{-12}s)$) we have the methods of molecular dynamics and density functional theory. This methods are appropriate for the study of transport coefficients and interaction potentials.

In this thesis we'll focus on the binary Phase Field Crystal (PFC) theory. The binary phase field crystal theory has been successful in describing a broad selection of phenomena in binary alloys. These successes include the Kirkendall effect [5, 26], solute drag [15], clustering and precipitation [9, 8, 7], colloidal ordering in drying suspensions [11], epitaxial growth and island formation [3, 27], and ordered crystals [1] to name a few.

The PFC theory is derived from Classical Density Functional Theory (CDFT) and as such it is a sort of simplified density functional theory. In practice, two different variants of the PFC theory are used in practice: The original model developed by Elder *et al* [4] and the Structural Phase Field Crystal (XPFC) model developed by Greenwood *et al.* [13]. The original model is a very reduced form of CDFT and so it lacks completeness in its ability to describe binary alloys. Specifically, the original model uses an expansion in concentration that limits its ability to describe a realistic phase diagram. The original model also uses a very simplified correlation kernel which limits its ability to describe a variety of crystal lattice structures. The XPFC model is an improvement in that is ameliorates both of these problems. The concentration is left unexpanded allowing for construction of realistic global phase diagrams instead of local expansions. The XPFC model provided a phenomenology for modelling correlation functions that succeeded in describing solidification of a variety of lattice structures (Find that paper about solidification of all 2d lattices).

In introducing its phenomenology for modelling correlation function, the XFPC theory tacitly assumes that there is some preferred structure at high concentration and some other

structure preferred at low concentration. This can be limited in situation that have a specific structure specifically at intermediate concentrations such a syntectic material. The XPFC model also assumes no long wavelength correlations in the concentration field which in practice means the model has an ideal free energy of mixing. This is another limitation of the XPFC model because in general the enthalpy of mixing is not zero for binary alloys.

This goal of the current research is to present two improvements to the binary XPFC theory. The first improvement is a more general phenomenology for modelling pair correlation functions of a material. The second improvement is two extend the free energy of mixing beyond ideality to account for circumstances when the heat of mixing is not negligible.

This thesis is divided into 6 chapters:

Chapter 2 Classical Density Functional Theory (CDFT) is introduced and derived from fundamental principles of quantum statistical mechanics.

Chapter 3 CDFT theory of solidification is described and discussed. The density functional theory is extended to a dynamic, non-equilibrium theory and the Phase Field Crystal (PFC) Theory is introduced as a simplified density functional theory.

Chapter 4 Binary PFC theory is established and previous simplified models are summarized and discussed.

Chapter 5 Improvements to the XPFC model are discussed and contains novel contribution to the field.

Chapter 6 Concludes the thesis by applying the improved XPFC model to the problem of multistep nucleation of nanoparticles and discusses potential future applications.

Chapter 2

Introduction to Classical Density Functional Theory

Many physical theories are derived using a succession of approximations. While each approximation yields a theory that is more narrow in scope, it is typically more tractible to either analytical or numerical analysis. Classical Density Functional Theory (CDFT) is derived using this approach and in this chapter we'll examine each approximation and the intermediate theory they supply.

CDFT is a theory of statistical mechanics. This means CDFT connects microscopic physics to macroscopic observables using statistical inference[1] instead of attempting to compute microscopic equations of motion. The microscopic physics in this case is most accurately described by many-body quantum mechanics and so the theory of quantum statistical mechanics is a natural starting point in any attempt to calculate thermodynamic observables.

We will see that for our systems of interest that the full quantum statistical theory is completely intractible. To preceed, we'll look at quantum statistical mechanics in the *semi-classical limit*. In the semi-classical limit we'll develop a theory of inhomogenous fluids called Classical Density Functional Theory (CDFT). Finally, we'll see that constructing exactly free

[1]Statistical mechanics is not always described as statistical inference. See works of E. T. Jaynes for details on this approach [19]

energy functionals for CDFT is rarely possible and look at an approximation scheme for these functionals.

2.1 Statistical Mechanics in the Semi-classical limit

At a microscopic level, all systems are governed by the fundamental physics of quantum mechanics. Statistical mechanics and in particular quantum statistical mechanics provides a map between this microscopic reality and macroscopic thermodynamic observables. For most applications, quantum statistical mechanics is both intractable to analysis and contains more detail than necessary. For instance, the precise bosonic or fermionic nature of the particles in the system often has little consequence on the thermodynamic properties. We can ignore some of these quantum mechanical details by looking at statistical mechanics in the *semi-classical limit*.

For the sake of clarity, we'll look at a system of N identical particles in the canonical ensemble which is straight forward to generalize to multi-component systems and other ensembles. We start with the definition of the partition function for a system of many particles,

$$Z = \mathrm{Tr}\left[e^{-\beta \hat{H}}\right], \tag{2.1}$$

where,

$\hat{H}$ is the Hamiltonian $\frac{|\hat{\mathbf{p}}|^2}{2m} + V(\hat{\mathbf{q}})$,

$\mathbf{p}$ is set of particle momenta $(p_1, p_2, ...p_N)$,

$\mathbf{q}$ is similarly the set of particles positions, and,

β is the inverse temperature $1/k_b T$ where k_b is the Boltzmann constant.

Wigner [35], and shortly after, Kirkwood [21] showed that the partition function could be expanded in powers of $\hbar$, facilitating the calculation of both a classical limit and quan-

tum corrections to the partition function. Their method, the Wigner-Kirkwood expansion, involves evaluating the trace operation over a basis of plane wave solutions,

$$\mathcal{Z}(\beta) = \int \frac{\mathrm{d}\mathbf{q}\mathrm{d}\mathbf{p}}{(2\pi\hbar)^N} e^{-\frac{i\mathbf{p}\cdot\mathbf{q}}{\hbar}} e^{-\beta\hat{H}} e^{\frac{i\mathbf{p}\cdot\mathbf{q}}{\hbar}} = \int d\Gamma I(\mathbf{q},\mathbf{p}), \tag{2.2}$$

Where, $d\Gamma$ is the phase space measure $\mathrm{d}\mathbf{p}\mathrm{d}\mathbf{q}/(2\pi\hbar)^N$. To compute the integrand, $I(\mathbf{q},\mathbf{p})$, we follow Uhlenbeck and Bethe [34] and first compute its derivative,

$$\frac{\partial I(\mathbf{q},\mathbf{p})}{\partial\beta} = -e^{\frac{i\mathbf{p}\cdot\mathbf{q}}{\hbar}} \hat{H} e^{-\frac{i\mathbf{p}\cdot\mathbf{q}}{\hbar}} I(\mathbf{q},\mathbf{p}). \tag{2.3}$$

We then make a change of variables, $I(\mathbf{q},\mathbf{p}) = e^{-\beta\mathcal{H}} W(\mathbf{q},\mathbf{p})$, where $\mathcal{H}$ is the classical Hamiltonian. The new function $W(\mathbf{q},\mathbf{p})$ encodes the deviation from classical behaviour due a lack of commutation of the potential and kinetic energy terms in the Hamiltonian. Using the explicit form of the quantum Hamiltonian and after a considerable amount of algebra we find a partial differential equation for W,

$$\frac{\partial W}{\partial\beta} = \frac{\hbar^2}{2}\left(\nabla^2_{\mathbf{q}} - \beta(\nabla^2_{\mathbf{q}}V) + \beta^2(\nabla V)^2 - 2\beta(\nabla_{\mathbf{q}}V)\cdot\nabla_{\mathbf{q}} + 2\frac{i}{\hbar}\mathbf{p}\cdot(\nabla_{\mathbf{q}} - \beta\nabla_{\mathbf{q}})\right) W(\mathbf{q},\mathbf{p}). \tag{2.4}$$

The solution can be written as a power series in $\hbar$, $W = 1 + \hbar W_1 + \hbar^2 W_2 + ...$ By plugging this expansion back into equation 2.1 we find a power series expansion for the partition function as well,

$$\mathcal{Z} = (1 + \hbar\langle W_1\rangle + \hbar^2\langle W_2\rangle + ...)\int d\Gamma e^{\beta\mathcal{H}}. \tag{2.5}$$

Where the average, $\langle\cdot\rangle$, denotes the the classical average,

$$\langle A(p,q)\rangle = \frac{1}{\mathcal{Z}}\int d\Gamma A(p,q) e^{-\beta\mathcal{H}}. \tag{2.6}$$

Solving equation 2.4 to second order in $\hbar$ and computing the classical averages in equation

2.5 the quantum corrections to the classical partition are computed to second order as[2],

$$\langle W_1 \rangle = 0, \tag{2.7}$$

$$\langle W_2 \rangle = -\frac{\beta^3}{24m} \left\langle |\nabla_{\mathbf{q}} V|^2 \right\rangle . \tag{2.8}$$

The first order term is zero because $W_1(\mathbf{q}, \mathbf{p})$ is an odd function of $\mathbf{p}$. In terms of the Helmholtz free energy, for example, the corrections to second order would be,

$$\mathcal{F} = \mathcal{F}_{classical} + \frac{\hbar^2 \beta^2}{24m} \left\langle |\nabla_{\mathbf{q}} V(\mathbf{q})|^2 \right\rangle . \tag{2.9}$$

There are a few items of importance in equation 2.9. First of all, the correction is inversely proportional to both the temperature and the particle mass. For copper at room temperature, for instance, the prefactor $\hbar^2\beta^2/(24m)$ is $\mathcal{O}(10^{-4})$ or at its melting temperature the prefactor is $\mathcal{O}(10^{-6})$. The correction is also proportional to the mean of the squared force felt by each particle. So high density materials will have a higher quantum correction because they sample the short-range repulsive region of the pair potential more than their low density counter parts.

2.1.1 Indistinguishability

There is an important distinction to be made between the quantum theory and the theory in the semi-classical limit. The integral over phase space of the partition function must only take into account the *physically different* states of the system. In the quantum theory this is achieved by tracing over any orthonormal basis of the Hilbert space, but in the classical theory we need to be careful not to double count states involving identical particle configurations. Classically, exchange of two identical particles does not result in a physically different state and thus these state should be considered only once in the sum over states in

[2]For detailed calculations see [24].

the partition function. More precisely, we should write the classical partition function as,

$$\mathcal{Z} = \int' d\Gamma e^{-\beta\mathcal{H}}, \tag{2.10}$$

Where the primed integral denotes integration only over the physically distinct states. In the common case of N identical particles, the phase space integral becomes,

$$\int' d\Gamma \to \frac{1}{N!}\int d\Gamma \tag{2.11}$$

Aggregating our results, we can write the partition function in the semi-classical limit as,

$$\mathcal{Z}(\beta) = \frac{1}{N!}\int d\Gamma e^{-\beta\mathcal{H}} + \mathcal{O}(\hbar^2), \tag{2.12}$$

Or, in the grand canonical ensemble,

$$\Xi(\mu,\beta) = \sum_{N=0}^{\infty} \frac{e^{\beta\mu N}}{N!}\int d\Gamma \left(e^{-\beta\mathcal{H}} + \mathcal{O}(\hbar^2)\right) \tag{2.13}$$

Of course, to first order in $\hbar$, this is exactly the form taught in introductory courses on statistical mechanics and derived by Gibbs[3] prior to any knowledge of quantum mechanics [12]. The key insight here is to understand, in a controlled way, when this approximation is accurate and the magnitude of the next quantum correction is as seen in equation 2.9. We now apply this semi-classical limit of statistical mechanics to the study of the local density field.

[3]The $\hbar$ in Gibbs' formula was justified on dimensional grounds and was simply a scaling factor with units of action $(J \cdot s)$

2.2 Classical Density Functional Theory

Ostensibly, when we study formation and evolution of microstructure in solids, our observable of interest is the density field. As per usual in theories of statistical thermodynamics we must distinguish between microscopic operators and macroscopic observables (the later being the ensemble average of the former). In classical statistical mechanics, operators are simply functions over the phase space, Γ. We use the term operator to make connection with the quantum mechanical theory. In the case of the density field, the microscopic operator is the sum of Dirac delta functions at the position of each particle,

$$\hat{\rho}(x;\mathbf{q}) = \sum_{i=0}^{N} \delta^{(3)}\left(x - q_i\right) \tag{2.14}$$

From which the thermodynamic observable is,

$$\rho(x) = \langle \hat{\rho}(x;\mathbf{q}) \rangle = \mathrm{Tr}\left[\hat{\rho}(x;\mathbf{q}) f(\mathbf{q},\mathbf{p})\right] \tag{2.15}$$

Where, $\mathrm{Tr}\left[\cdot\right]$ now denotes the classical trace,

$$\mathrm{Tr}\left[A(\mathbf{q},\mathbf{p}) f(\mathbf{q},\mathbf{p})\right] \equiv \sum_{N=0}^{\infty} \frac{1}{N!} \int \mathrm{d}\Gamma A(\mathbf{q},\mathbf{p}) f(\mathbf{q},\mathbf{p}), \tag{2.16}$$

And, $f(\mathbf{q},\mathbf{p})$ is the equilibrium probability density function,

$$f(\mathbf{q},\mathbf{p}) = \frac{e^{-\beta(\mathcal{H}-\mu N)}}{\Xi(\mu,\beta)}. \tag{2.17}$$

To construct a theory of the density field we review the usual methodology for statistical thermodynamics. We will do so in the frame of entropy maximization in which the entropy is maximized subject to the macroscopically available information. Taking the existance of a average of the density field, particle number and energy as the macroscopically available

information, we can maximize the entropy functional,

$$S[f(\mathbf{q},\mathbf{p})] = -k_b \mathrm{Tr}\left[f(\mathbf{q},\mathbf{p}) \ln\left(f(\mathbf{q},\mathbf{p})\right)\right], \tag{2.18}$$

subject to the aforementioned contraints to find a probability density function of the form,

$$f(\mathbf{q},\mathbf{p}) \propto \exp\left\{-\beta\left(\mathcal{H} - \mu N + \int \mathrm{d}x \phi(x)\hat{\rho}(x)\right)\right\}. \tag{2.19}$$

Where, β, μ and $\phi(x)$ are the Lagrange multipliers associated with constraints of average energy, number of particles and density respectively. As you might imagine, the constraints of average particle number and density are not independent and with the insight that,

$$N = \int dx \hat{\rho}(x), \tag{2.20}$$

We can combine their Lagrange multipliers into one,

$$f(\mathbf{q},\mathbf{p}) \propto \exp\left(-\beta(\mathcal{H} - \int \mathrm{d}x \psi(x)\hat{\rho}(x))\right), \tag{2.21}$$

Where, $\psi(x) = \mu - \phi(x)$, is the combined Lagrange multiplier named the *intrinsic chemical potential*. Recalling that chemical potential is the change Helmholtz free energy made by virtue of adding particles to the system,

$$\frac{\partial F}{\partial N} = \mu, \tag{2.22}$$

The interpretation of the intrinsic chemical potential follows as the Helmholtz free energy change due to particles being added to a specific location. We'll see this in more detail briefly where we'll see a analogous equation for the intrinsic chemical potential.

The objective of statistical theories to compute the statistics of some observable (random variable) of choice. Two special sets of statistics provide a complete description of

the observable's probability distribution: the *moments* and *cumulants*[4]. The calculation of moments and cumulants can be aided by use of generating functions. In the case of statistical mechanics the generating functions of moments and cumulants have special physical significance. The generating function of moments is closely related to the partition function and the generating function of cumulants is closely related to the associated thermodynamic potential.

In the case where the observable is local density field, this is made somewhat more technical by the fact that the density is an entire function instead of a scalar variable. As such the partition function is more precisely called the partition *functional* as it depends on an entire function of input. The thermodynamic potential will also be a functional. Specifically, the grand canonical partition functional is,

$$\Xi[\psi(x)] = \mathrm{Tr}\left[\exp\left(-\beta\mathcal{H} + \beta\int \mathrm{d}x\psi(x)\hat{\rho}(x)\right)\right]. \tag{2.23}$$

As eluded to above, the partition functional is a type of moment generating functional in the sense that repeated (functional) differentiation yields moments of the density field:

$$\frac{\beta^{-n}}{\Xi}\frac{\delta^n\Xi[\psi]}{\delta\psi(x_1)\dots\delta\psi(x_n)} = \langle\hat{\rho}(x_1)\dots\hat{\rho}(x_n)\rangle\,. \tag{2.24}$$

Similarly, we can construct a thermodynamic potential by taking the logarithm of the partition function. This potential in particular is called the *grand potential functional* in analogy with the grand potential of thermodynamics,

$$\Omega[\psi(x)] = -k_bT\log\left(\Xi[\psi(r)]\right). \tag{2.25}$$

The grand potential functional is a type of cumulant generating functional in the sense that

[4]See [23] for discussion of moments, cumulants and their importance in statistical mechanics

repeated functional differentiation yields cumulants of the density field:

$$-\frac{\beta^{-n+1}\delta^n\Omega[\psi]}{\delta\psi(x_1)\dots\delta\psi(x_n)} = \langle\hat{\rho}(x_1)\dots\hat{\rho}(x_n)\rangle_c \tag{2.26}$$

Where, $\langle\cdot\rangle_c$, denotes the cumulant average [23].

If we examine the first two cumulants,

$$-\frac{\delta\Omega[\psi]}{\delta\psi(x)} = \langle\hat{\rho}(x)\rangle \equiv \rho(x), \tag{2.27}$$

$$-k_bT\frac{\delta^2\Omega[\psi]}{\delta\psi(x)\delta\psi(x')} = \langle(\hat{\rho}(x)-\rho(x))(\hat{\rho}(x')-\rho(x'))\rangle\,, \tag{2.28}$$

We notice something remarkable: The first, implies that the average density field is a function of only its conjugate field, the intrinsic chemical potential, and the second implies that that relationship is invertible[5]. To see this, we compute the Jacobian by combining equation 2.27 and 2.28,

$$\frac{\delta\rho(x)}{\delta\psi(x')} = \beta\,\langle(\hat{\rho}(x)-\rho(x))(\hat{\rho}(x')-\rho(x'))\rangle\,. \tag{2.29}$$

The right hand side of equation 2.29 is an autocorrelation function and therefore positive semi-definite by Weiner-Khinchin theorem. This implies that, at least locally, the intrinsic chemical potential can always be written as a functional of the average density, $\psi[\rho(x)]$, and vice versa. Furthermore, because all of the higher order cumulants of the density depend on the intrinsic chemical potential, they too depend only on the average density.

Given the importance of the average density, $\rho(x)$, if follows that we would like to use a thermodynamic potential with a natural dependence on the density. We can construct a generalization of the Helmholtz free energy that has precisely this characteristic by Legendre

[5]The inverse function theorem only implies local invertibility, there is no guarentee of global invertibility. Indeed phase coexistance is a manifestation of this fact where a single intrinsic chemical potential is shared by two phases

transforming the Grand potential,

$$\mathcal{F}[\rho(x)] = \Omega[\psi[\rho]] + \int dx \rho(x)\psi(x). \tag{2.30}$$

$\mathcal{F}[\rho(x)]$ is called the *intrinsic free energy functional*.

It can be shown [16] that $\rho(x)$ must be the global minimum of the grand potential, which sets the stage for the methodology of classical density functional theory: if we have a defined intrinsic free energy functional, $\mathcal{F}$, we can find the equilibrium density field by solving the asssociated Euler-Lagrange equation,

$$\frac{\delta\Omega[\rho]}{\delta\rho(r)} = 0. \tag{2.31}$$

Finally, we may construct an analogous equation to equation 2.22 for the intrinsic chemical potential,

$$\frac{\delta\mathcal{F}}{\delta\rho(x)} = \psi(x). \tag{2.32}$$

Equation 2.32 implies that the intrinsic chemical potential is the free energy cost of adding density to the location x specifically.

2.3 Techniques in Density Functional Theory

The difficulty in formulating a density functional theory is the construction of an appropriate free energy functional. While exact calculations are rarely feasible, there are a variety of techniques that help in building approximate functionals. Its important to note first what we *can* compute exactly. In the case of the ideal gas, we can compute the grand potential

and free energy functional exactly,

$$\Omega_{id}[\psi] = -\frac{k_b T}{\Lambda^3} \int \mathrm{d}x\, e^{\beta\psi(x)} \tag{2.33}$$

$$\mathcal{F}_{id}[\rho] = k_b T \int \mathrm{d}x \left\{ \rho(x) \ln\left(\Lambda^3 \rho(x)\right) - \rho(x) \right\}, \tag{2.34}$$

Where Λ is the thermal de Broglie wavelength,

$$\Lambda = \sqrt{\frac{2\pi\hbar^2}{m k_b T}}. \tag{2.35}$$

We may then express a deviations from ideality by factoring the ideal contribution out of the partition function,

$$\Xi[\psi] = \Xi_{id}[\psi]\Xi_{ex}[\psi], \tag{2.36}$$

leading to grand potential and free energy functionals split into ideal and *excess* components,

$$\Omega = \Omega_{id} + \Omega_{ex} \tag{2.37}$$

$$\mathcal{F} = \mathcal{F}_{id} + \mathcal{F}_{ex}. \tag{2.38}$$

The interaction potential, $V(\mathbf{q})$, in the excess partition function typically makes a direct approach to calculating the excess free energy intractible. Though perturbative methods, including the cluster expansion technique [29], have been developed to treat the interaction potential systematically, other approximation schemes for the excess free energy are typically more pragmatic. In particular, we can approximate the excess free energy by expanding around a reference homogeneos fluid with chemical potential μ_0 and density ρ_0,

$$\mathcal{F}_{ex}[\rho] = \mathcal{F}_{ex}[\rho_0] + \left.\frac{\delta \mathcal{F}_{ex}}{\delta\rho(x)}\right|_{\rho_0} * \Delta\rho(x) + \frac{1}{2}\Delta\rho(x') * \left.\frac{\delta^2 \mathcal{F}_{ex}}{\delta\rho(x)\delta\rho(x')}\right|_{\rho_0} * \Delta\rho(x) + \ldots, \tag{2.39}$$

Where $\Delta\rho(x) = \rho(x) - \rho_0$ and we have introduced the notation, $*$ to mean integration over

repeated co-ordinates,

$$f(x') * g(x') \equiv \int \mathrm{d}x' f(x')g(x'). \tag{2.40}$$

The excess free energy is the generating functional of family of correlation functions called *direct correlation functions*,

$$\frac{\delta^n \mathcal{F}_{ex}[\rho]}{\delta\rho(x_1)...\delta\rho(x_n)} = -\beta C^n(x_1, \ldots, x_n). \tag{2.41}$$

The first of which, for a uniform fluid, is the excess contribution to the chemical potential which we may express as the total chemical potential less the ideal contribution,

$$\left.\frac{\delta F_{ex}}{\delta\rho}\right|_{\rho_0} = \mu_0^{ex} = \mu_0 - \mu_{id} = \mu_0 - k_b T \ln\left(\Lambda^3\rho_0\right). \tag{2.42}$$

Truncating the expansion in equation 2.39 to second order in $\Delta\rho(x)$ and substitute the linear and quadratic terms with equation 2.42 and 2.41 we can simplify the excess free energy to,

$$\mathcal{F}_{ex}[\rho(r)] = \mathcal{F}_{ex}[\rho_0] + \int dr \left\{\mu - k_b T \ln\left(\Lambda^3\rho_0\right)\right\} \Delta\rho(r) - \frac{k_b T}{2}\Delta\rho(r) * C_0^{(2)}(r, r') * \Delta\rho(r') \tag{2.43}$$

Combining equation 2.34 with the simplified excess free energy in equation 2.43, we can express total change in free energy, $\Delta\mathcal{F} = \mathcal{F} - \mathcal{F}[\rho_0]$, as,

$$\Delta\mathcal{F}[\rho(r)] = k_b T \int \mathrm{d}r \left\{\rho(r) \ln\left(\frac{\rho(r)}{\rho_0}\right) - (1 - \beta\mu_0)\Delta\rho(r)\right\} - \frac{k_b T}{2}\Delta\rho(r) * C_0^{(2)}(r, r') * \Delta\rho(r'). \tag{2.44}$$

We find an equivalent expression for the grand potential after a Legendre transform,

$$\Delta\Omega[\rho(r)] = k_b T \int \mathrm{d}r \left\{\rho(r) \left[\ln\left(\frac{\rho(r)}{\rho_0}\right) + \beta\phi(r)\right] - \Delta\rho(r)\right\} - \frac{k_b T}{2}\Delta\rho(r) * C_0^{(2)}(r, r') * \Delta\rho(r'). \tag{2.45}$$

Its reasonable to ask at this point whether or not we have really gained anything with this approximation scheme. Although we have arrived at a relatively simple form for the free

energy functional, we've added a lot of parameters to the functional based on the reference fluid. Thankfully, the theory of homogeneous liquids, such as our reference liquid, is very well established. This means we may relay on a broad choice of analytical, numerical or experimental techniques to derive these parameters.

Equation 2.44 establishes an approximate density functional theory for inhomogenous fluids and, as we will see in the following chapter, for the seemingly disparate phenonmena of solidification. We see that it can derived through a series of approximations from a fundamental basis in quantum statistical mechanics and requires no more parameters than the thermodynamic details of a homogeneous reference fluid.

Chapter 3

Classical Density Functional Theory of Freezing

The classical density functional theories derived in chapter 2 was first established to study inhomogenous fluids. By considering the solid state as an especially extreme case of an inhomogeneous fluid [17], we can use CDFT to study the process of solidification. From the perspective of CDFT, solidification occurs once the density field develops long range periodic solutions. While not expressed in precisely this language, this approach dates back as far as 1941 with the early work of Kirkwood and Monroe [22] and was later significantly refined by Youssof and Ramakrishnan [32].

We'll see that the approach of Youssof and Ramakrishnan was very successful at explaining the solidification in the thermodynamic sense. That is to say, it elucidate the parameters responsible for solidification but not the dynamical pathway responsible for the transition. To discuss the pathway to equilibrium and the non-equilibrium artifacts it introduces into many solids (grain boundaries, vacancies, dislocations etc) we proceed to extend the CDFT framework using the Dynamic Density Functional Theory (DDFT). Noting that the full DDFT framework can be cumbersome in practice we conclude by introducing a simplified density functional theory called the Phase Field Crystal (PFC) theory.

3.1 Amplitude Expansions

To explore the problem of solidification, we begin with the approximate grand potential established in equation 2.45 with the external potential, $\phi(r)$, set to zero,

$$\beta\Delta\Omega[\rho(r)] = \int dr \left\{ \rho(r) \ln\left(\frac{\rho(r)}{\rho_0}\right) - \Delta\rho(r) \right\} - \frac{1}{2}\Delta\rho(r) * C_0^{(2)}(r, r') * \Delta\rho(r'). \tag{3.1}$$

To make our theory concrete we must choose a suitable reference liquid to set the parameters ρ_0 and $C_0^{(2)}(r, r')$. We will choose the reference liquid to be the liquid at the melting point with density ρ_l.

Scaling out a factor of ρ_l we can rewrite the grand potential in terms of a dimensionless reduced density, $n(r) \equiv (\rho(x) - \rho_l)/\rho_l$,

$$\frac{\beta\Delta\Omega[n(r)]}{\rho_l} = \int dr \left\{ (1 + n(r)) \ln(1 + n(r)) - n(r) \right\} - \frac{1}{2} n(r) * \rho_l C_0^{(2)}(r, r') * n(r'). \tag{3.2}$$

To describe the density profile in the solid state we can expand the density in a plane waves,

$$n(r) = \bar{n} + \sum_{\mathbf{G}} \xi_{\mathbf{G}} e^{i\mathbf{G}r}. \tag{3.3}$$

Where, $\{\mathbf{G}\}$, is the set of reciprocal lattice vectors in the crystal lattice and the amplitudes, $\xi_{\mathbf{G}}$, serve as order parameters for freezing. In the liquid phase all amplitudes are zero and the average density is uniform, while in the solid phase there are finite amplitudes that describe the periodic profile of the crystal lattice. By design, $\bar{n}$ is zero for the liquid phase at the melting point and $\bar{n}$ is the fractional density change of solidification, η for the solid phase at the melting point. Where,

$$\eta = \frac{\rho_s - \rho_l}{\rho_l}, \tag{3.4}$$

In which ρ_s is the macroscopic density of the solid phase.

The amplitudes are constrained by the point group symmetry of the lattice. Grouping

the amplitudes of symmetry-equivalent reciprocal lattice vectors together we can write the density profile as,

$$n(r) = \bar{n} + \sum_{\alpha} \left\{ \xi_\alpha \sum_{\{\mathbf{G}\}_\alpha} e^{i\mathbf{G}\cdot\mathbf{x}} \right\}, \tag{3.5}$$

Where α is a label running over sets of symmetry-equivalent reciprocal lattice vectors.

If we insert equation 3.5 into equation 3.2 and integrate over the unit cell we find,

$$\begin{aligned} \frac{\beta\Delta\Omega_{cell}}{\rho_l} = & \int_{cell} dr \left\{ (n(r)+1)\ln\left(n(r)+1\right) - n(r) \right\} \\ & - \frac{1}{2}\left[\bar{n}^2 \rho_l \tilde{C}_0^{(2)}(0) + \sum_{\alpha} \rho_l \tilde{C}_0^{(2)}(\mathbf{G}_\alpha)\lambda_\alpha |\xi_\alpha|^2 \right], \end{aligned} \tag{3.6}$$

Where λ_α is the number of reciprocal lattice vectors in the set α and $\tilde{C}_0^{(2)}(k)$ is the Fourier transform of the direct correlation function of the reference fluid. The first term in equation 3.6 is convex in all of the amplitudes with a minimum at zero. It is noteworthy, as we will see discuss shortly, that the product $\rho_l \tilde{C}_0^{(2)}(\mathbf{G}_\alpha)$ is a simple function of the structure factor, $S(k)$[1] ,

$$\rho\tilde{C}(k) = \frac{S(k)-1}{S(k)} \quad \forall\ k \neq 0. \tag{3.7}$$

It follows that solidification must occur when the product $\rho_l \tilde{C}_0^{(2)}(\mathbf{G}_\alpha)$ (or equivalently, the reference structure factor $S_0(\mathbf{G}_\alpha)$) is large enough to stabilize a finite amplitude by creating a new minimum away from zero. This phenomena is shown schematically in figure 3.1 where the grand potential is projected on to a particular ξ_α axis and plotted for different values of the reference structure factor.

[1]This follows from the definition of the structure factor and the Ornstein-Zernike equation

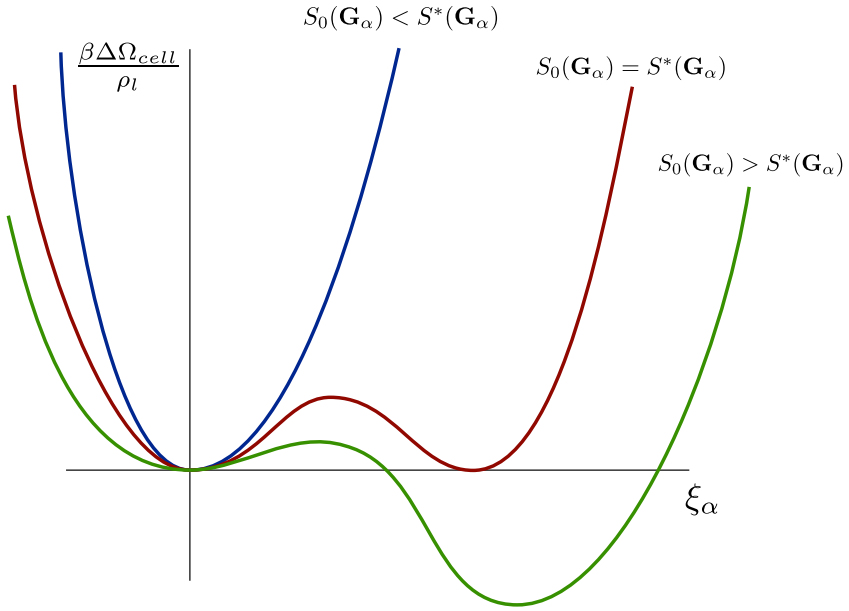

Figure 3.1: Schematic view of the grand potential $\beta\Delta\Omega/\rho_l$ projected on to the ξ_α axis for a three different reference structure factors. To minimize the grand potential, finite ξ_α is stable once $S_0(\mathbf{G}_\alpha) > S^*(\mathbf{G}_\alpha)$

Furthermore, equation 3.6 suggests that the set of critical structure factors, $\{S^*(\mathbf{G}_\alpha)\}_\alpha$ are material independent as free parameters remain in the grand potential. As a consequence, once we specify the symmetry of the lattice a liquid will solidify into (eg. face-centred-cubic), all materials that undergo this transition should share these parameters at the melting point.

Early numerical evidence of this result was supplied by the Hansen-Verlet criterion [18] which states that for Lennard-Jones fluid the peak of the structure factor is constant along the melting curve with a value ≈ 2.85. It has been noted that in aggregating experimental evidence many liquids solidifying to fcc structure have a peak value close to 2.8 whereas those solidifying into bcc structures have a peak value around 3.0 [32].

At this level, the CDFT theory of solidification is an infinite order parameter theory of solidification. We can simplify the theory by truncating the number of amplitudes we keep in our expansion of the density. This is justified by noting that only a few reciprocal lattice families contain the majority of the grand potential energy of solidification. As seen in table 3.1a and table 3.1b theoretical results from a single amplitude theory (theory I in the

results) are poor but improve significantly with two order parameters (theory II) or higher order expansions of the free energy (theory III).

Theory	$\tilde{C}(\mathbf{G}_{[111]})$	$\tilde{C}(\mathbf{G}_{[311]})$	$\bar{n}$
I	0.95	0.0	0.074
II	0.65	0.23	0.270
III	0.65	0.23	0.166
Experiment	0.65	0.23	0.148

(a) Freezing parameters for fcc with comparison to Argon experimental results.

Theory	$\tilde{C}(\mathbf{G}_{[110]})$	$\tilde{C}(\mathbf{G}_{[211]})$	$\bar{n}$
I	0.69	0.00	0.048
II	0.63	0.07	0.052
III	0.67	0.13	0.029
Experiment	0.65	0.23	0.148

(b) Freezing parameter for bcc with comparison to Sodium experimental results.

Table 3.1: Freezing parameters for fcc and bcc systems and comparison to experiment from [32]. Theory I uses one order parameter, theory II uses two order parameter and theory III uses two order parameters with a higher (third) order expansion in the free energy. η is the fraction density change of solidification from equation 3.4

3.2 Dynamic Density Functional Theory

In spite of its successes the CDFT theory of solidification cannot be a general description of solidification as many materials never fully reach equilibrium. The resulting microstructure affects the mechanical properties of the solid. In order to improve our theory we need to examine the pathway systems take to equilibrium so we can understand these microstructural features. We begin with a brief overview of non-equilibrium statistical mechanics.

3.2.1 Overview of Non-equilibrium Statistical Mechanics

Consider a non-equilibrium probability distribution over phase space, $f(\mathbf{q}, \mathbf{p}; t)$. As a function over phase space, its equation of motion is a simple result of classical mechanics,

$$\frac{df}{dt} = \{f, \mathcal{H}\} + \frac{\partial f}{\partial t}. \tag{3.8}$$

Where, $\{\cdot,\cdot\}$, denotes the Poisson bracket,

$$\{f,g\} = \sum_{i=0}^{N} \frac{\partial f}{\partial q_i}\frac{\partial g}{\partial p_i} - \frac{\partial g}{\partial q_i}\frac{\partial f}{\partial p_i}. \tag{3.9}$$

Of course, the distribution must remain normalized in time and therefore the total time derivative must be zero,

$$\int d\mathbf{q}d\mathbf{p}\, f(\mathbf{q},\mathbf{p};t) = 1 \rightarrow \frac{df}{dt} = 0. \tag{3.10}$$

Accounting for this conservation law in equation 3.8, the resulting equation of motion is called the *Liouville Equation*,

$$\frac{\partial f}{\partial t} = -\{f,\mathcal{H}\} \tag{3.11}$$

Under appropriate conditions the probability distribution, under the action of the Liouville Equation, will decay to a stable fixed point $f_{eq}(\mathbf{q},\mathbf{p})$ we call equilibrium,

$$\lim_{t\to\infty} f(\mathbf{q},\mathbf{p};t) = f_{eq}(\mathbf{q},\mathbf{p}) \tag{3.12}$$

Using the non-equilibrium probability distribution, we can also discuss non-equilibrium averages of the density profile and their associated equations of motions. The non-equilibrium density is written in analogy with equation 2.15 by taking of the classical trace of the density operator over with the non-equilibrium distribution,

$$\rho(x,t) = \langle\hat{\rho}(x;\mathbf{q})\rangle_{ne} = \mathrm{Tr}\left[\hat{\rho}(x;\mathbf{q})f(\mathbf{q},\mathbf{p},t)\right]. \tag{3.13}$$

Where, $\langle\cdot\rangle_{ne}$, denotes the non-equilibrium average. Just as the non-equilibrium probability distribution is driven to equilibrium by the Liouville Equation, so too is the density profile by its own equation of motion.

3.2.2 Equations of Motion

A variety of equations of motion for the density field are known. For instance, we can consider the Navier-Stokes equations of hydrodynamics as one such equation of motion. If we restrict ourselves to diffusion limited circumstances, we may derive a much simplier equation of motion. To acheive this result we use the projection operator method, and assume that the density operator is the only relevant variable. Quoting the result from [6] we find,

$$\frac{\partial \rho(r,t)}{\partial t} = \nabla \cdot \left[\int \mathrm{d}r' \, \mathbf{D}(r,r',t) \cdot \nabla' \frac{\delta \mathcal{F}[\rho]}{\delta \rho(r',t)} \right], \tag{3.14}$$

Where, $\mathbf{D}(r,r',t)$, is the diffusion tensor,

$$\mathbf{D}(r,r',t) = \int_0^\infty \mathrm{d}\tau' \, \mathrm{Tr} \left[f(\mathbf{q},\mathbf{p},t) \hat{\mathbf{J}}(r,0) \hat{\mathbf{J}}(r',\tau') \right], \tag{3.15}$$

in which $\hat{\mathbf{J}}(r,t)$ is the density flux is,

$$\hat{\mathbf{J}}(r,t) \equiv \sum_i^N \frac{p_i}{m_i} \delta(r - q_i). \tag{3.16}$$

Theories using equation and variations there of are often called *Dynamic Density Functional Theories* (DDFT) or at times *Time Dependent Density Functional Theories* (TDDFT) though we will use the former throughout this work.

The non-equilibrium diffusion tensor presents a significant impedement to integrating this equation of motion so in practice the diffusion tensor is often approximated. Following [6], if we assume that the positions evolve more slowly than the velocities and that the momenta of different particles are uncorrelated we can dramatically simplify the diffusion tensor,

$$D(r,r') = D_0 \mathbb{1} \rho(r,t) \delta(r - r'). \tag{3.17}$$

Where D_0 is diffusion coefficient,

$$D_0 = \frac{1}{3m^2}\int_0^\infty \mathrm{d}t \mathrm{Tr}\left[f(\mathbf{q},\mathbf{p},t)p_i \cdot p_i(t)\right]. \tag{3.18}$$

Substituting into equation 3.14 we find a simplified equation of motion originally suggested by [28],

$$\frac{\partial \rho(r,t)}{\partial t} = \nabla \cdot \left[D_0 \rho(r,t) \nabla \frac{\delta \mathcal{F}[\rho]}{\delta \rho(r,t)}\right]. \tag{3.19}$$

The equation of motion can also be written as a Langevin equation. In this variant the equation of motion is for the density *operator*, $\hat{\rho}$, and the noise is assumed to obey a generalized Einstein relation,

$$\frac{\partial \hat{\rho}(x,t)}{\partial t} = \nabla \cdot \left[D_0 \hat{\rho}(x,t) \nabla \left(\frac{\delta \mathcal{F}[\hat{\rho}]}{\delta \hat{\rho}}\right)\right] + \xi(x,t), \tag{3.20}$$

$$\langle \xi(x,t) \rangle = 0, \tag{3.21}$$

$$\langle \xi(x,t)\xi(x',t') \rangle = -2\nabla \cdot \left[D_0 \rho(x,t) \nabla \delta(x-x')\delta(t-t')\right]. \tag{3.22}$$

See Appendix **??** for more details on generalized Einstein relations and [2] for a detailed discussion about equations 3.19 and 3.20.

At times the diffusion tensor is assumed to be constant. This is common place in many Phase Field Crystal theories. In light of equation 3.19, this is akin to assuming the density variations are small.

Unfortunately, if we were to use the approximate free energy functional established in equation 2.44 in the dynamic density functional theory of equation 3.19 or 3.20 we would face a major impedement: the solid state solutions of the density functional theory approach yield sharply peaked solutions at the position of the atoms in the lattice. While this is realistic, they are a major challenge for numerical algorithms. The challenges are two-fold. First, these sharp peaks require a fine mesh to be resolved resulting in large memory requirement to simulate domains of any non-trivial scale. Second, lineary stability analysis of most

algorithms demonostrates that the time step size is a monotonic increasing function of the grid spacing so only small time steps can be taken on a fine mesh.

One pragmatic solution to this problem is to further approximate the free energy functional of equation 2.44 in such a way as to produce a theory that retains the essential physics of solidification but produces a solid state that is more smoothly peaked. As we will see next, the Phase Field Crystal (PFC) theory acheives precisely this balance.

3.3 Phase Field Crystal Theory

The phase field crystal theory (PFC) presents a solution to the numerical difficulties faced by DDFT methods by approximating the free energy in such a way as to retain the basic features of the theory with a smoother solid state solution. Starting with the approximate free energy functional of equation 2.44 we proceed as previously by scaling out a factor of the reference density and changing variables to a dimensionless density $n(r) = (\rho(r) - \rho_l)/\rho_l$,

$$\frac{\beta\mathcal{F}[n(r)]}{\rho_l} = \int dr \left\{(n(r)+1)\ln(n(r)+1) - (1-\beta\mu)n(r)\right\} - \frac{1}{2}n(r) * \rho_l C_0^{(2)}(r,r') * n(r'). \tag{3.23}$$

We then Taylor expand the logarithm about the reference density or equivalently $n(r) = 0$, to fourth order,

$$\frac{\beta\mathcal{F}[n(r)]}{\rho_l} = \int dr \left\{\frac{n(r)^2}{2} - \frac{n(r)^3}{6} + \frac{n(r)^4}{12}\right\} - \frac{1}{2}n(r) * \rho_l C_0^{(2)}(r,r') * n(r'). \tag{3.24}$$

Where the linear term has been dropped because it leaves the equations of motion invariant. Most phase field crystal theories also use a simplified equation of motion as well,

$$\frac{\partial n(r,t)}{\partial t} = M\nabla^2\left(\frac{\delta\mathcal{F}[n(r)]}{\delta n(r)}\right). \tag{3.25}$$

Chapter 4

Simplified Binary Phase Field Crystal Models

In this chapter we will walk through three simplified binary PFC models. The first is the original binary PFC model, which, while highly successful at modelling a few important phenomena is ultimately limited in scope. The second is the binary structural phase field crystal, or binary XPFC which was successful in modelling a broad spectrum of crystalline structures, but was limited in its ability of model liquid instablilities and a variety of phase diagrams. Finally, we'll see a new contribution to which we will call the regular phase field crystal model which is successful in modeling a broad spectrum of invariant binary reactions and crystalline structures.

All binary PFC models begin with a multicomponent variant of the approximate free energy functional established in Chapter 2,

$$\beta\mathcal{F}[\rho_A,\rho_B] = \sum_{i=A,B}\int \mathrm{d}r\,\rho_i(r)\ln\left(\frac{\rho_i(r)}{\rho_i^0}\right) - (1-\beta\mu_i^0)\Delta\rho_i(r) \\ -\frac{1}{2}\sum_{i,j=A,B}\Delta\rho_i(r) * C_{ij}^{(2)}(r,r') * \Delta\rho_j(r'). \tag{4.1}$$

It is convenient to change variables to a dimensionless total density, $n(r)$ and local concen-

tration, $c(r)$,

$$n(r) = \frac{\Delta\rho}{\rho_0} = \frac{\Delta\rho_A + \Delta\rho_B}{\rho_A^0 + \rho_B^0} \tag{4.2}$$

$$c(r) = \frac{\rho_B}{\rho} = \frac{\rho_B}{\rho_A + \rho_B}. \tag{4.3}$$

Scaling out a factor of the total reference density, ρ_0 we can break the free energy functional in these new variables into three parts,

$$\frac{\beta\mathcal{F}[n,c]}{\rho_0} = \frac{\beta\mathcal{F}_{id}[n]}{\rho_0} + \frac{\beta\mathcal{F}_{mix}[n,c]}{\rho_0} + \frac{\beta\mathcal{F}_{ex}[n,c]}{\rho_0}, \tag{4.4}$$

Where,

$$\frac{\beta\mathcal{F}_{id}[n]}{\rho_0} = \int \mathrm{d}r \, \left\{(n(r)+1)\ln(n(r)+1) - (1-\beta\mu^0)n(r)\right\} \tag{4.5}$$

$$\frac{\beta\mathcal{F}_{mix}[n,c]}{\rho_0} = \int \mathrm{d}r \, \left\{(n(r)+1)\left(c\ln\left(\frac{c}{c_0}\right) + (1-c)\ln\left(\frac{1-c}{1-c_0}\right)\right)\right\}, \tag{4.6}$$

And, if we assume the local concentration $c(r)$ varies over much longer length scales than the local density $n(r)$,

$$\begin{aligned}\frac{\beta\mathcal{F}_{ex}[n,c]}{\rho_0} = &-\frac{1}{2}n(r) * [C_{nn}(r,r') * n(r') + C_{nc}(r,r') * \Delta c(r')] \\ &-\frac{1}{2}\Delta c(r) * [C_{cn}(r,r') * n(r') + C_{cc}(r,r') * \Delta c(r')]\,.\end{aligned} \tag{4.7}$$

We have introduced μ_0 as the total chemical potential of the reference mixture, $c_0 = \rho_B^0/\rho_0$ as the reference concentration and $\Delta c(r) = c(r) - c_0$ as the deviation of the concentration

from the reference. The $n - c$ pair correlation introduced in the excess free energy are,

$$C_{nn} = \rho_0 \left(c^2 C_{BB} + (1-c)^2 C_{AA} + 2c(1-c) C_{AB} \right) \tag{4.8}$$

$$C_{nc} = \rho_0 \left(c C_{BB} - (1-c) C_{AA} + (1-2c) C_{AB} \right) \tag{4.9}$$

$$C_{cn} = C_{nc} \tag{4.10}$$

$$C_{cc} = \rho_0 \left(C_{BB} + C_{AA} - 2C_{AB} \right) \tag{4.11}$$

Explicit calculations can be found in Appendix **??**. Differences in the various simplified binary PFC theories stem from differing approximations of the terms in the free energy stated in equation 4.4.

4.1 Original Binary Phase Field Crystal Model

In the original simplified binary PFC theory, all terms in the free energy are expanded about $n(r) = 0$ and $c(r) = c_0$ (ie., about their reference states). For the ideal free energy this results in a polynomial truncated to fourth order,

$$\frac{\beta \mathcal{F}_{id}[n]}{\rho_0} = \int \mathrm{d}r \left\{ \frac{n(r)^2}{2} - \frac{n(r)^3}{6} + \frac{n(r)^4}{12} \right\}. \tag{4.12}$$

The linear term is dropped due to invariance in the equations of motion. If we assume for simplicity of demonstration $c_0 = 1/2$, the free energy of mixing becomes a simple fourth order polynomial as well,

$$\frac{\beta \mathcal{F}_{mix}[n, c]}{\rho_0} = \int \mathrm{d}r \left\{ 2\Delta c(r)^2 + \frac{4\Delta c(r)^4}{3} \right\}. \tag{4.13}$$

Linear couplings to $n(r)$ are dropped by assuming, as we already have, that the concentration field varies on a much longer length scale than the total density and noting that the total density is defined about its average. This argument can also be applied the linear couplings

to $n(r)$ in the excess free energy term which leaves only the C_{nn} and C_{cc} terms. Finally, these two terms are approximated with a gradient expansions of the correlation functions,

$$C_{nn}(r, r') = \delta(r - r') \left(\alpha + \beta\nabla^2 + \gamma\nabla^4 + \ldots\right), \tag{4.14}$$

$$C_{cc}(r, r') = \delta(r - r') \left(\epsilon + \xi\nabla^2 + \ldots\right). \tag{4.15}$$

The expansion parameters, α, β, and γ are all dependent on temperature and concentration. We are required to expand C_{nn} to fourth order because, as noted in chapter **??** the peak of the direct correlation function in Fourier space is the driving force for solidification. The concentration field is correlated over a longer length scale implying that only the short wavevectors are important in C_{cc} so we can expand just to quadratic order.

Gathering terms the resulting free energy functional for the original simplified binary PFC model[1] is,

$$\begin{aligned}\frac{\beta\mathcal{F}[n, c]}{\rho_0} = &\int \mathrm{d}r \left\{\frac{1}{2}n(r)\left(1 - \alpha - \beta\nabla^2 - \eta\nabla^4\right)n(r) - \frac{n(r)^3}{6} + \frac{n(r)^4}{12}\right\} \\ &+ \int \mathrm{d}r \left\{\frac{1}{2}\Delta c(r)\left(4 - \epsilon - \xi\nabla^2\right)\Delta c(r) + \frac{4\Delta c(r)^4}{3}\right\}.\end{aligned} \tag{4.16}$$

The strength of the original simplified binary PFC model is that is retains most of the important physics of binary alloys in a very reduced theory. For instance, the simplified model is capable of describing the equilibrium phase diagrams of both eutectic alloys alloys and materials with a solid state spinodal / liquid minimum. Supplied with a diffusive equation of motion the simplified model can model an impressive diversity of dynamic phenomena including eutectic growth, phase segregation, dendritic growth, dislocation motion in solid state spinodal coarsening and epitaxial growth.

The major limitation of the original simplified model is that the gradient expansion of the density-density correlation function gives only a crude control over the structures that

[1]The orignal simplified binary PFC model was expressed using slightly different variables. We expand in $\Delta c(r)$ here to facilitate comparison with other theories

will be formed. In fact, as this theory only controls a single peak in Fourier space it can only solidify into the fcc phase [check this is the case for the original theory]. As noted in chapter **??**. The ability to solidify into an arbitrary structure demands control of value of the density-density correlation function at all reciprocal lattice vectors.

A second limitation of the original simplified model is that it is local in concentration. This means that realistic phase diagrams from 0 to 100% concentration cannot be produced, only local phase diagrams around the reference concentration that was expanded about. To construct these global phase diagrams we require the entire free energy of mixing term in equation 4.6.

4.2 Binary Structural Phase Field Crystal Model

The binary structural phase field crystal theory (XPFC) seeks to remedy the two short comings of the original simplified model. That is, it seeks to construct realistic phase diagrams for binary systems and seeks to reproduce a variety of crystal lattice structure. We'll begin with a derivation of the theory and compare with the original model.

First, the ideal free energy is expanded in precisely the same manner resulting in the same fourth order polynomial,

$$\frac{\beta\Delta\mathcal{F}_{id}[n]}{\rho_0} = \int \mathrm{d}r \left\{ \frac{n(r)^2}{2} - \eta\frac{n(r)^3}{6} + \chi\frac{n(r)^4}{12} \right\}. \qquad \text{(4.12 revisited)}$$

The free energy of mixing is left unexpanded but an overall scale ω is added to fit the mixing term away from the reference concentration,

$$\frac{\beta\mathcal{F}_{mix}[n,c]}{\rho_0} = \int \mathrm{d}r \left\{ \omega(n(r)+1)\left(c\ln\left(\frac{c}{c_0}\right) + (1-c)\ln\left(\frac{1-c}{1-c_0}\right)\right)\right\}. \qquad (4.17)$$

This unexpanded free energy of mixing will lead to more accurate global phase diagrams. The excess free energy is approximated using the similar assumptions as in the original model

(linear couplings are dropped), but the density-density correlation function is not expanded. Greenwood *et al* all assumed that the $k = 0$ mode of the concentration-concentration correlation function was zero leaving only the quadratic term in the expansion,

$$C_{cc}(r, r') = \delta(r - r')\alpha\nabla^2. \tag{4.18}$$

Grouping terms together, the complete free energy functional for the binary XPFC model is,

$$\begin{aligned}\frac{\beta\Delta\mathcal{F}[n, c]}{\rho_0} = &\int \mathrm{d}r \left\{\frac{1}{2}n(r)\left(1 - C_{nn}(r, r')\right) * n(r') - \eta\frac{n^3}{6} + \chi\frac{n^4}{12}\right\} \\ &+ \int \mathrm{d}r \left\{\frac{1}{2}\left|\nabla c(r)\right|^2 + \omega f_{mix}(r)\right\}.\end{aligned} \tag{4.19}$$

Where $f_{mix}(r)$ is the local free energy density of mixing,

$$f_{mix}(r) = (n(r) + 1)\left(c(r)\ln\left(\frac{c(r)}{c_0}\right) + (1 - c(r))\ln\left(\frac{1 - c(r)}{1 - c_0}\right)\right). \tag{4.20}$$

4.2.1 Modelling Correlation Functions

The key insight made by the XPFC model the that, the density-density correlation function can be modelled in such a way as to control the crystall lattice structure targetted under cooling and to target different structures at different concentrations. Note that the density-density correlation function as the form of a linear combination of interpolating functions in concentration, $\zeta(c)$, multiplied by bare correlation functions $C(r, r')$,

$$C_{nn}(r, r'; c) = \sum_i \zeta_i(c)C_i(r, r') \tag{4.21}$$

In the exact theory, for example, we have,

$$\zeta_{AA}(c) = \rho_0(1 - c^2), \tag{4.22}$$

$$\zeta_{AB}(c) = \rho_0 c(1 - c), \tag{4.23}$$

$$\zeta_{BB}(c) = \rho_0 c^2. \tag{4.24}$$

Each interpolating function, $\zeta_i(c)$, defines a domain of validity for its associated correlation function $C_i(r, r')$. This suggests that we might model any density-density correlation function using this general structure: the set of correlation function $C_i(r, r')$ enumerate the various structures that may manifest themselves and the associated interpolation functions $\zeta_i(c)$ define the concentrations over which these correlations are valid.

As a simple example we wanted to construct a simple model of the silver-cupper eutectic alloy system, we might start with some model correlation function for pure silver, $C_\alpha(r, r')$, and for pure copper, $C_\beta(r, r')$. These two structures, the silver rich α phase and the copper rich β phase, are the only two relevent crystalline structures in the system so to build the full density-density correlation function we just need to choose interpolating functions for each. Following Greenwood *et al* for example, we might choose,

$$\zeta_\alpha(c) = 1 - 3c^2 + 2c^3, \tag{4.25}$$

$$\zeta_\beta(c) = 1 - 3(1 - c)^2 + 2(1 - c)^3. \tag{4.26}$$

This leaves the question of how to develop model correlation functions for any particular crystalline lattice of interest. This problem is also anwsered by the XPFC framework. Originally delineated for pure systems, the XPFC method for constructing correlation functions is strongly influenced by the methods developed by Ramakrishnan. In particular this means that, given that the driving force for solidification is the of value direct correlation function at the reciprocal lattice vectors, we need a model correlation function that controls these

parameters specifically. We can acheive this with Gaussian peaks centred at the reciprocal lattice vector positions,

$$C_i(r, r') = \sum_{\alpha} e^{\frac{T}{T_i^0}} e^{-\frac{(k-k_i)^2}{2\sigma_i^2}} \tag{4.27}$$

Where, as in chapter **??**, the index α runs over families of point group equivalent reciprocal lattice vectors. The temperature dependent prefactors e^{T/T_i^0} give the correct temperature scaling of the amplitudes close to the melting point[2] as discussed by [1].

The advantages of the XPFC simplified binary model are two fold: realistic phase diagrams and modelling a variety of crystalline lattices. While the former is relatively cosmetic the latter allows for the examination of guininely novel systems in comparison with the original simplified model. For example the binary XPFC model as been used to study, peritectic systems, ordered crystals, [find refs and list of applications] [14, 1].

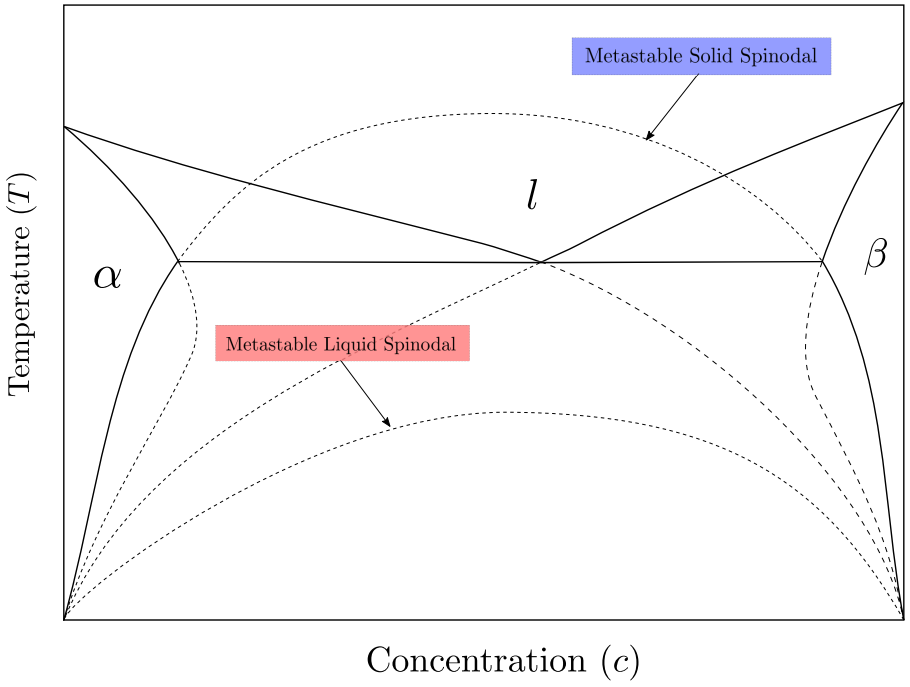

Figure 4.1: Eutectic phase diagram with metastable projects. Stable coexistance lines are rendered solid where as metastable projections are dashed.

Unfortunately, by assuming that the $k = 0$ mode of the concentration-concentration

[2]The original XPFC works used a phenomonological prefacter with e^{T^2/C_i} for a constant C_i. This choice is inspired by harmonic analysis in the solid phase and the Debye-Waller factor

correlation function is zero the XPFC model restricts the its free energy of mixing to an ideal model of mixing. This model of mixing includes only entropic contributions to the free energy. This means that the sole driving force for phase seperation is elastic energy as the heat of mixing is always positive (right? I always mess up this convention). This can be a limitation on modelling a variety of binary alloy systems, for instance both monotectic and syntectic systems cannot be modelled without a negative heat of mixing. More subtly, even eutectic systems have a negative heat of mixing deep below the eutectic point as the metastable liquid has a spinodal. This phenomena is shown shown schematically in figure 4.1 where the metastable projections, including solid and liquid spinodals, are drawn on a hypothetical eutectic phase diagram. Problems such as the stability of nanocrystalline binary alloys require an examination of the balance of elastic energies and bulk mixing free energy [30].

Conclude the chapter with discussion of where what we've seen and lead into the discussion for the next chapter of dynamics and applications of this theory to more than just simple equilibrium phase diagrams

Chapter 5

Improvements to the Binary XPFC Model

5.0.1 Modelling Correlation Functions

The key insight made by the XPFC model the that, the density-density correlation function can be modelled in such a way as to control the crystall lattice structure targetted under cooling and to target different structures at different concentrations. Note that the density-density correlation function as the form of a linear combination of interpolating functions in concentration, $\zeta(c)$, multiplied by bare correlation functions $C(r, r')$,

$$C_{nn}(r, r'; c) = \sum_i \zeta_i(c) C_i(r, r') \tag{5.1}$$

In the exact theory, for example, we have,

$$\zeta_{AA}(c) = \rho_0(1 - c^2), \tag{5.2}$$

$$\zeta_{AB}(c) = \rho_0 c(1 - c), \tag{5.3}$$

$$\zeta_{BB}(c) = \rho_0 c^2. \tag{5.4}$$

Each interpolating function, $\zeta_i(c)$, defines a domain of validity for its associated correlation function $C_i(r, r')$. This suggests that we might model any density-density correlation function using this general structure: the set of correlation function $C_i(r, r')$ enumerate the various structures that may manifest themselves and the associated interpolation functions $\zeta_i(c)$ define the concentrations over which these correlations are valid.

As a simple example we wanted to construct a simple model of the silver-cupper eutectic alloy system, we might start with some model correlation function for pure silver, $C_\alpha(r, r')$, and for pure copper, $C_\beta(r, r')$. These two structures, the silver rich α phase and the copper rich β phase, are the only two relevent crystalline structures in the system so to build the full density-density correlation function we just need to choose interpolating functions for each. Following Greenwood *et al* for example, we might choose,

$$\zeta_\alpha(c) = 1 - 3c^2 + 2c^3, \tag{5.5}$$

$$\zeta_\beta(c) = 1 - 3(1-c)^2 + 2(1-c)^3. \tag{5.6}$$

The regular phase field crystal model is a simplified model that aims to combine the positive aspects of the XPFC and original simplified models together. The original PFC model uses an regular model of mixing so both enthalpic and entropic contribution to the free energy of mixing are considered. This is acheived by assuming there is a $k = 0$ contribution in the gradient expansion of the concentration-concentration correlation function. If we add this simple component to the development of the XPFC free energy functional we find one additional term that gives an enthaly of mixing,

$$\begin{aligned} \frac{\beta \Delta \mathcal{F}[n, c]}{\rho_0} = &\int \mathrm{d}r \left\{ \frac{1}{2} n(r) \left(1 - C_{nn}(r, r')\right) * n(r') - \eta \frac{n^3}{6} + \chi \frac{n^4}{12} \right\} \\ &+ \int \mathrm{d}r \left\{ \frac{1}{2} \left|\nabla c(r)\right|^2 + \omega f_{mix}(r) \right\}. \end{aligned} \tag{5.7}$$

Where the local free energy density of mixing, f_{mix} is now,

$$f_{mix}(r) = (n(r)+1)\left(c(r)\ln\left(\frac{c(r)}{c_0}\right) + (1-c(r))\ln\left(\frac{1-c(r)}{1-c_0}\right)\right) + \frac{1}{2}\epsilon(c-c_0)^2. \quad (5.8)$$

The simplicity the temperature dependence if the parameter ϵ is taken to be linear about the spinodal temperature T_c,

$$\epsilon(T) = -4 + \epsilon_0(T - T_c). \quad (5.9)$$

5.0.2 Equilibrium Properties

Here we'll explore the flexibility of the simplified regular PFC model in describing various material phase diagrams in binary systems.

Eutectic Phase Diagram

While previous PFC models have shown that elastic energy is a sufficient driving force for eutectic solidification our simplified regular model allows for the examination of the role enthalpy of mixing can play in eutectic solids. For instance, Murdoch and Schuh noted that in nanocrystalline binary alloys, while a positive enthaply of segregation can stabilize against grain growth via solute segregation at the grain boundary, if the enthaply of mixing becomes too large this effect can be negated by second phase formation or even macroscopic phase seperation[30].

To specialize our simplified regular model to the case of the binary eutectic we must choose an appropriate model for the correlation function. Choosing an α phase around $c = 0$ and β phase around $c = 1$, we can recover the pair correlation function used in the binary

XPFC with a particular choice of window functions:

$$\zeta_\alpha(c) = 2c^3 - 3c^2 + 1 \tag{5.10}$$

$$\zeta_\beta(c) = \zeta_\alpha(1-c). \tag{5.11}$$

Should we choose, for example, an α and β phase with 2 dimensional hexagonal lattices, differing only by lattice constants, we can produce a phase diagram like that in Fig. 5.1.

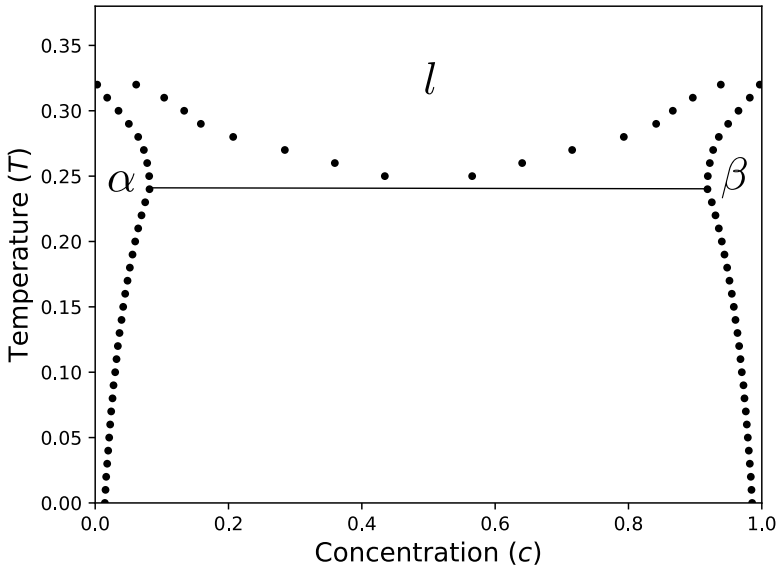

Figure 5.1: Eutectic phase diagram triangle α and β phases. The free energy parameter are $\eta = 2$, $\chi = 1$, $\omega = 0.30$, $\epsilon_0 = 3$ and $T_c = 0.01$. The parameters of the structure functions are $\alpha_{10\alpha} = \alpha_{10\beta} = 0.8$, $k_{10\alpha} = 2\pi$, $k_{10\beta} = 4\pi/\sqrt{3}$ and $T_0 = 1$

Syntectic Phase Diagram

Our regular model also allows for the study of a variety of invariant binary reactions that, to date, have not been studied using phase field crystal models. One such reaction is the syntectic reaction.

The syntectic reaction, $l_1 + l_2 \rightarrow \alpha$, consists of solidification at the interface of two liquids. We can achieve this with our model by setting the spinodal temperature, T_c, sufficiently high

and producing a density-density correlation function that is peaked at a concentration below the spinodal. This can be done by choosing a window function that is centered about an intermediate concentration, c_α of the solid phase, α.

$$\chi(c) = e^{-\frac{(c-c_\alpha)^2}{2\alpha_c}} \tag{5.12}$$

The resulting correlation function for a hexagonal lattice in two dimensions, for example, would be,

$$\tilde{C}_{nn}(k;c) = e^{-\frac{(c-c_\alpha)^2}{2\alpha_c}} e^{-\frac{T}{T_0}} e^{-\frac{(k-k')^2}{2\alpha^2}} \tag{5.13}$$

A phase diagram that produces a syntectic reaction with an appropriate choice of parameters can be seen in Fig. 5.2.

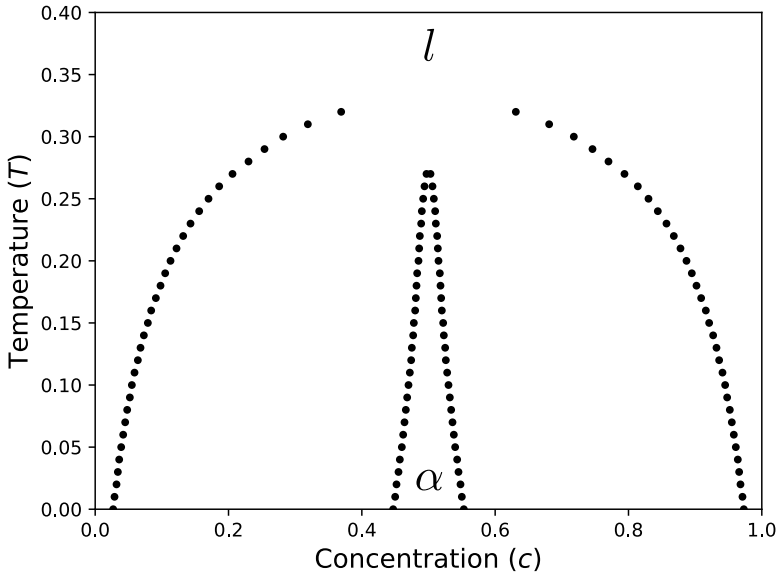

Figure 5.2: Phase Diagram of Syntectic Alloy with a hexagonal α phase. The free energy parameters are $\eta = 2$, $\chi = 1$, $\omega = 0.3$, $\epsilon_0 = 10$ and $T_c = 0.35$. The parameters for the structure function are $\alpha_{10\alpha} = 0.8$, $k_{10\alpha} = 2\pi$ and $T_0 = 1$

Monotectic Phase Diagram

The monotectic reaction is another invariant binary reaction that has not previously been studied using PFC models. The monotectic reaction, $l_1 \rightarrow \alpha + l_2$, consists of decomposing liquid into a solute poor solid and solute rich liquid. To model a monotectic using our regular model we hypothesize a solid phase at $c = 0$ and set the spinondal temperature higher than the solidification temperature. To achieve this we use a window function peaked around $c = 0$,

$$\chi_\alpha(c) = e^{-\frac{c^2}{2\alpha_c^2}}. \tag{5.14}$$

Again considering a simple hexagonal lattice for the α phase, we can produce a phase diagram with a monotectic reaction with an appropriate choice of parameters as in Fig. 5.3.

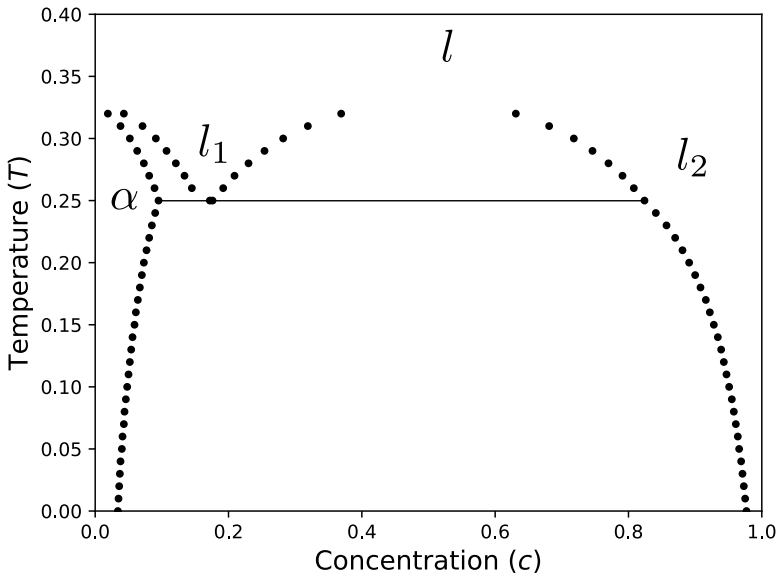

Figure 5.3: Phase Diagram of Monotectic Alloy with hexagonal α phase. The free energy parameters are $\eta = 2$, $\chi = 1$, $\omega = 0.3$, $\epsilon_0 = 10$, $T_c = 0.35$ and $c_0 = 0.75$. The parameters for the structure function are $\alpha_{10\alpha} = 0.8$, $k_{10\alpha} = 2\pi$ and $T_0 = 1$ and the parameter for the window function is $\alpha_c = 0.4$

Precipitation from Solution

We can also model precipitation of nanoparticles from solution. While on its surface the equilibrium phase diagram of a solution is that of a simple solid-liquid coexistance, in practice the metastable features of the phase diagram can have profound implications on the nucleation kinetics of precipitate. As an example, precipitation from solution is a typical synthesis technique for gold and silver nanoparticles. Recent work by Loh *et al* shows that a metastable spinodal may be playing an important role in the growth and nucleation of gold nanoparticles under certain diffusive circumstances.

Using the regular XPFC model we can reproduce the condition of a metastable liquid spinodal underneath the liquid-solid coexistance curve. The approach to produce a phase diagram is the same as that of of a monotectic, with the exception that the spinodal temperature, T_c, most now be sufficiently low to be buried underneath the coexistance curve. In keeping with the concentration being that of the solute, we'll also center the gaussian window function about $c = 1$. An example, including metastable spinodal, can be seen in Fig. 5.4.

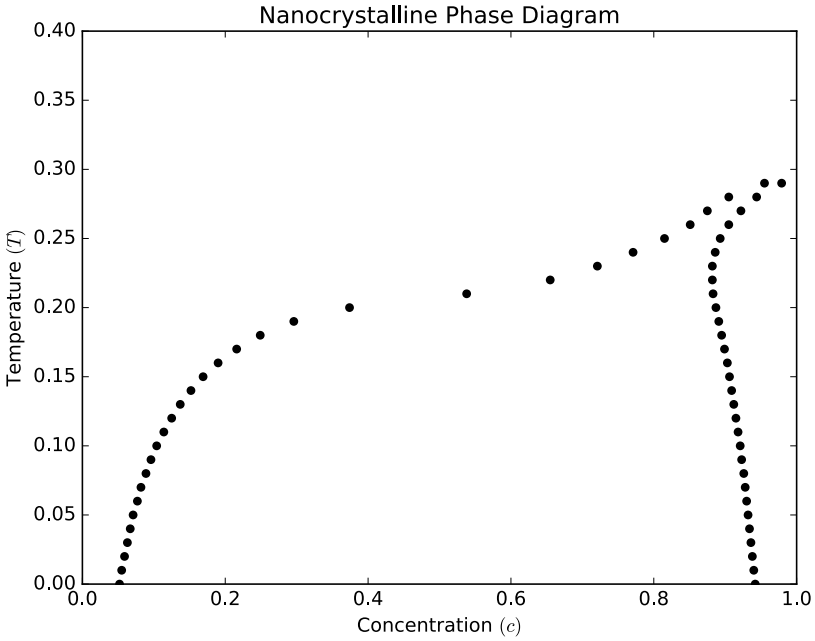

Figure 5.4: Phase Diagram of Solution fill me in please!!

Conclude the chapter with discussion of where what we've seen and lead into the discussion for the next chapter of dynamics and applications of this theory to more than just simple equilibrium phase diagrams

Chapter 6

Applications

In this chapter we discuss applications of our improvements to the binary XPFC model. To begin we'll discuss an effective equation of motion in the limit that density change on solidification is small, after which we'll examine the to process of multi-step nucleation of nanoparticles from solution. To conclude we'll discuss areas of future application.

6.0.1 Dynamics

To examine applications of our improvements to the XPFC model we begin by considering equations of motion. Following [13], we use conservative dynamics for both $n(x,t)$ and $c(x,t)$.

$$\frac{\partial n(x,t)}{\partial t} = M_n \nabla^2 \left(\frac{\delta \beta \Delta \mathcal{F}/\rho_0}{\delta n(x,t)} \right) + \xi_n(x,t), \tag{6.1}$$

$$\frac{\partial c(x,t)}{\partial t} = M_c \nabla^2 \left(\frac{\delta \beta \Delta \mathcal{F}/\rho_0}{\delta c(x,t)} \right) + \xi_c(x,t). \tag{6.2}$$

These equations of motion are largely phenomenological as, strictly speaking, there is no reason that the local concentration should be conserved. This conservation can be justified in the limit that the total density does not deviate far from the reference. When this is the case we have $c \equiv \rho_B/\rho \approx \rho_B/\rho_0$ which *is* conserved.

6.1 Multistep Nucleation of Nanoparticles in Solution

Recent experimental work has shown that gold and silver nanoparticles follow a pathway vary different from that assumed by Classical Nucleation Theory (CNT). Loh *et al.* showed that these nanoparticles precipitate first via spinodal decomposition of the aqueous solution followed by nucleation inside the resulting gold-rich fluid. CNT assumes that, for binary systems, assumes that changes in order and composition occur simultaneously.

This is one example among many works that point to a deficiency in CNT. Common among these works is the presence of a multi-step nucleation process. While some theoretical description exist for these multi-step processes, they typically posit highly simplified pathways to nucleation for simplicity of analysis that may be far from the actual kinetics experienced by the system. For instance in the study of condensation of a pure material, [cite Duran-Olivencia] restricted the nucleus to a spherical droplet with radius R and density ρ. Thus restricted, they find that the most likely path to nucleation follows a three-stage pathway. These theories can justify a multi-step nucleation pathway but do little more to advance our knowledge of the *actual* pathway to nucleation.

It is important, then, to have robust models that contain all of the essential physics of these systems to gain a deeper insight into the phenomena. The works of Loh [cite] are a special case of diffusion limited precipitation because their system was a 30nm thick aqueous solution. The effective diffusion constant in this thin water film is 9 orders of magnitude smaller than in the bulk and as such the system is diffusion limited. To model this process we must be able to model changes in composition, structure and density. A negative enthalpy of mixing is clearly playing in important role so our improved XPFC model is a good fit.

To construct an appropriate free energy functional for this system we consider the structure of its equilibrium phase diagram. Precipitation is indicative of a simple liquid-solid coexistance curve beneath which we assume there must also be a metastable liquid spinodal. Producing a system with these characteristics is similar to that of a monotectic with the exception that the spinodal temperature, T_c, must now be sufficiently low to hide below

the coexistance curve. We will also also use a Gaussian window function $\zeta(c)$ as the in the monotectic case though this time centring the Gaussian about $c = 1$ in keeping with interpretting the concentration as a solute concentration. An example, including depiction of the metastable spinodal, can be seen in figure 6.1.

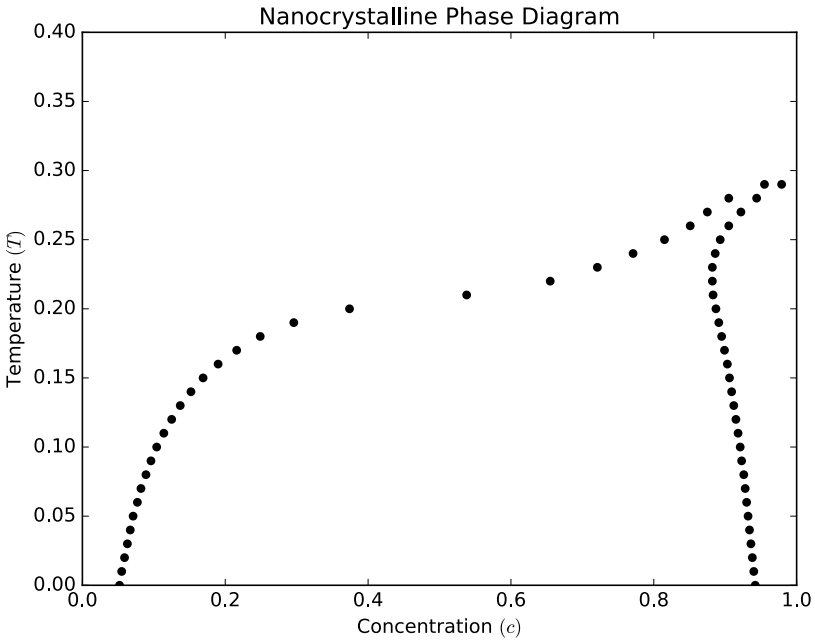

Figure 6.1: Phase Diagram of Solution fill me in please!!

We would expect that, starting from a uniform initial condition, if we quench the system through the coexistance region and past the liquid spinodal we might see a nucleation pathway similar to that observed experimentally. Results of a numerical simulation [1] can be seen in figure **??**. We see that, much as in experimental observation, nanoparticle nucleation is preceeded by spinodal decomposition.

[1] See appendix D for a detailed description of the integration algorithm

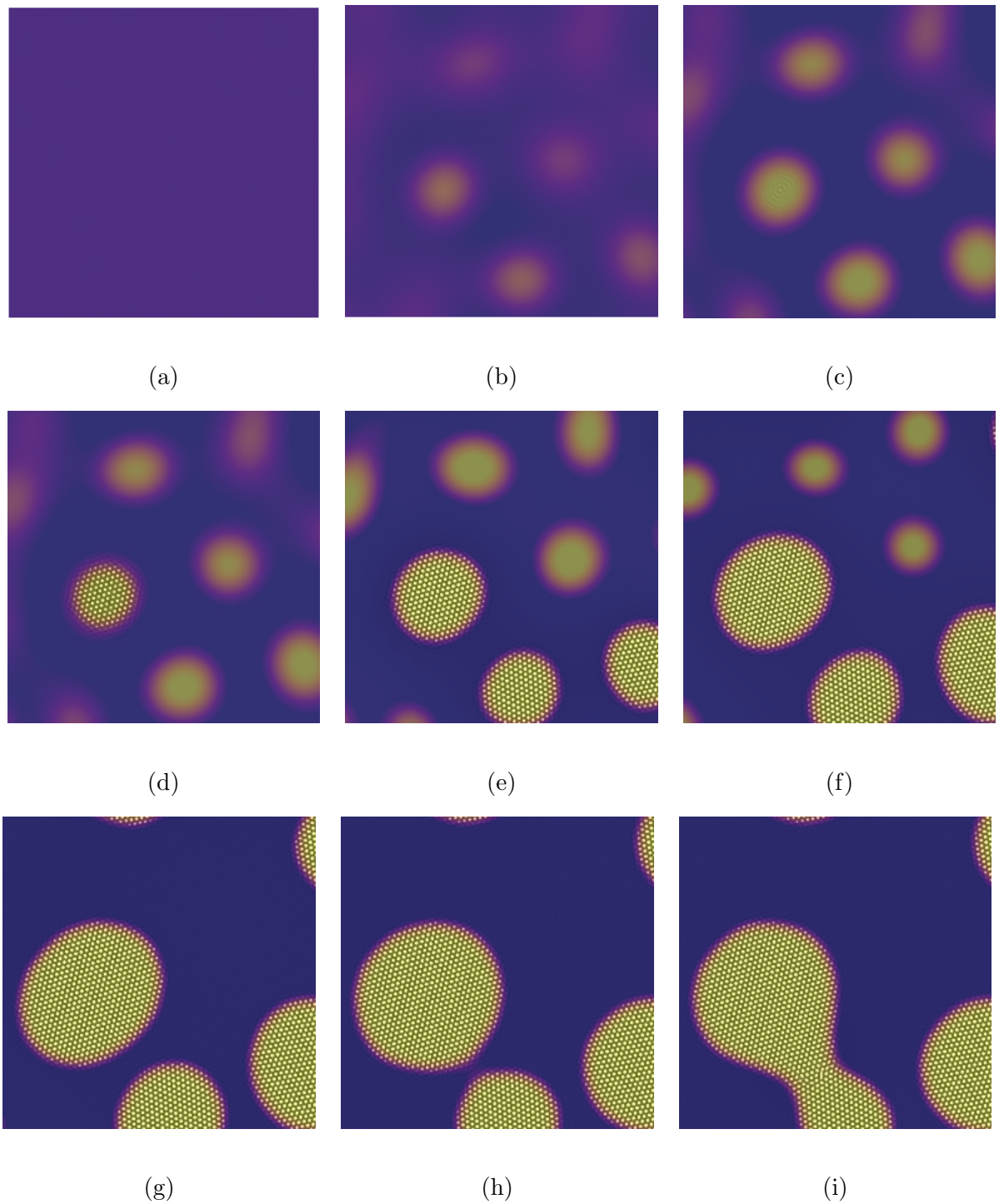

Figure 6.2: Various stages of precipitation of nanoparticles from solution. All thermodynamic parameters are shared with figure 6.1. The initial condition is a uniform solution quenched abruptly to $T = 0.07$. The initial condition has concentration $c = 0.3$ and relative density $n = 0.05$. Mobilities M_n and M_c are set to 1 and W_c is set to 3.0. Numerical parameters are grid spacing $\Delta x = 0.125$ on a 1024 by 1024 lattice with time step size $\Delta t = 0.0025$. Sub-figures (a) - (c) show spinodal decomposition of the liquid into solute right and solute poor regions. Sub-figures (d) - (f) show nucleation of the solid and solid growth at the expense of liquid regions. The remaining sub-figures show only nanoparticle growth and coarsening.

Our model finds some addition complexity in the nucleation process as well. Once crystalline nuclei start to form, they growth is accelerated at the expense of the solute-rich liquid droplets in solution. In a system of coarsen droplets with only a single phase, larger droplets grow at the expense of smaller droplets to reduce the total surface tension in the system. This process is called Oswald ripening. In the nanoparticle system even smaller crystalline particles can grow at the expense of larger liquid droplets due to their difference in chemical potential.

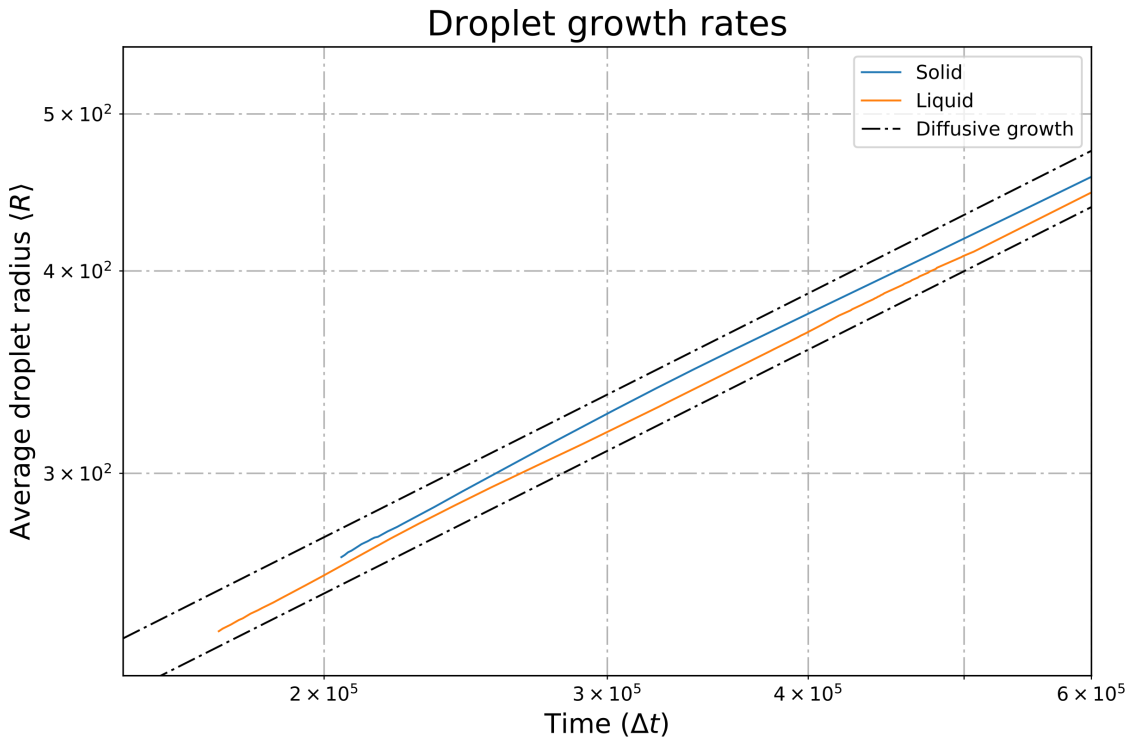

Figure 6.3: Droplet growth exponents

We can examine this growth phenomena more systematically by measuring the ensemble average droplet radius $\langle R(t) \rangle$ over time. We achieve this by running 120 simulations with the same parameters as the quench described in figure **??** and computing the radius of all droplets and their phase (liquid or solid) throughout the simulation. Strictly diffusive

growth scales like $\langle R(t) \rangle \sim t^{1/2}$ and so in plotting the mean radius versus time on a log-log plot as in figure **??** we see how the growth of solid and liquid droplets compare to diffusive growth. Early solid droplets grow at a slightly hyper-diffusive rate due to the presence of the sacrificial liquid droplets and slow to sub-diffusive as they begin to coarsen.

Appendix A

Noise in Nonlinear Langevin Equations

When using Langevin equations to study non-equilibrium statistical mechanics, the noise strength can be linked to the transport coefficients through a generalization of the Einstein relation. The generalization was first developed by Onsager and Machlup [31]. The typical strategy for deriving such a relationship is to evaluate the equilibrium pair correlation function by two separate methods: the equilibrium partition functional and the equation of motion[1].

While the equilibrium partition functional gives pair correlation through the typical statistical mechanical calculation, the equation of motion can be used to derive a dynamic pair correlation function that must be equal to the equilibrium pair correlation function in the long time limit.

In what follows we'll look at how to formulate a generalized Einstein relation from a generic Langevin equation and then calculate two specific examples using Model A dynamics and a ϕ^4 theory and Time Dependent Density Functional Theory (TDDFT) and a general Helmholtz free energy.

[1]For considerations far from equilibrium see [25, 33, 10]

A.1 Generalized Einstein Relations in an Arbitrary Model

We start by considering a set of microscopic observables, $a_i(r,t)$, that are governed by a nonlinear Langevin equation,

$$\frac{\partial \mathbf{a}(r,t)}{\partial t} = F[\mathbf{a}(r,t)] + \boldsymbol{\xi}(r,t). \tag{A.1}$$

Where, $\mathbf{a}$, denotes a vector of our fields of interest. These microscopic equation of motion may have been derived from linear response, projection operators or some other non-equilibrium formalism. We assume that the random driving force, $\boldsymbol{\xi}(r,t)$ is unbaised, Gaussian noise that is uncorrelated in time.

$$\langle \boldsymbol{\xi}(r,t) \rangle = 0 \tag{A.2}$$

$$\left\langle \boldsymbol{\xi}(r,t)\boldsymbol{\xi}^{\dagger}(r',t') \right\rangle = \mathbf{L}(r,r')\delta(t-t') \tag{A.3}$$

We wish to constrain the form of the covariance matrix, $\mathbf{L}$, by demanding that the solution to the Langevin equation eventually decays to equilibrium and that correlations in equilibrium are given by Boltzmann statistics.

We begin by linearizing the equation of motion about an equilibrium solution, $\mathbf{a}(r,t) = \mathbf{a}_{eq}(r) + \hat{\mathbf{a}}(r,t)$.

$$\frac{\partial \hat{\mathbf{a}}(r,t)}{\partial t} = \mathbf{M}(r,r') * \hat{\mathbf{a}}(r',t) + \boldsymbol{\xi}(r,t) \tag{A.4}$$

Where, $*$ denotes an inner product and integration over the repeated variable. eg:

$$\mathbf{M}(r,r') * \hat{\mathbf{a}}(r') = \sum_j \int dr' M_{ij}(r,r')\hat{a}_j(r'). \tag{A.5}$$

We can formally solve our linearized equation of motion,

$$\hat{\mathbf{a}}(r,t) = e^{\mathbf{M}(r,r')t} * \hat{\mathbf{a}}(r',0) + \int_0^t d\tau\, e^{\mathbf{M}(r,r')(t-\tau)} * \boldsymbol{\xi}(r',\tau), \tag{A.6}$$

And use this formal solution to evaluate the dynamic pair correlation function.

$$\left\langle \hat{\mathbf{a}}(r,t)\hat{\mathbf{a}}^{\dagger}(r',t')\right\rangle = e^{\mathbf{M}(r,r_1)t} * \left\langle \hat{\mathbf{a}}(r_1,0)\hat{\mathbf{a}}^{\dagger}(r_2,0)\right\rangle * e^{\mathbf{M}^{\dagger}(r',r_2)t'} + \int_0^t \int_0^{t'} d\tau d\tau' \, e^{\mathbf{M}(r,r_1)(t-\tau)} * \left\langle \boldsymbol{\xi}(r_1,0)\boldsymbol{\xi}^{\dagger}(r_2,0)\right\rangle * e^{\mathbf{M}^{\dagger}(r',r_2)(t'-\tau')} \tag{A.7}$$

To evaluate the equilibrium correlation function we take the limit as each time goes to infinity together ($t = t' \to \infty$). It is important to note that every eigenvalue of $\mathbf{M}$ must be negative for our solution to decay to equilibrium in the long time limit (eg. $lim_{t\to\infty}\hat{\mathbf{a}}(r,t) = 0$) and as such the first term in our dynamic correlation function won't contribute to the equilibrium pair correlation. This is as we might expect as the first term holds the contributions to the dynamic correlation function from the initial conditions. The second term can be evalutated by substituting the noise correlation and evaluating the delta function.

$$\mathbf{\Gamma}(r,r') = \lim_{t\to\infty} \left\langle \hat{\mathbf{a}}(r,t)\hat{\mathbf{a}}^{\dagger}(r',t)\right\rangle = \int_0^{\infty} dz \, e^{\mathbf{M}(r,r_1)z} * \mathbf{L}(r_1,r_2) * e^{\mathbf{M}^{\dagger}(r',r_2)z} \tag{A.8}$$

Considering the product $\mathbf{M}(r,r_1) * \mathbf{\Gamma}(r_1,r')$ and performing an integration by parts gives the final generalized Einstein relation.

$$\mathbf{M}(r,r_1) * \mathbf{\Gamma}(r_1,r') + \mathbf{\Gamma}(r,r_1) * \mathbf{M}^{\dagger}(r_1,r') = -\mathbf{L}(r,r') \tag{A.9}$$

A.2 Example 1 - Model A

As a first example of calculating an Einstein relation consider the following free energy functional under non-conservative, dissipative dynamics.

$$\beta\mathcal{F}[\phi] = \int dr \left\{ \frac{1}{2}|\nabla\phi(x)|^2 + \frac{r}{2}\phi^2(x) + \frac{u}{4!}\phi^4(x) + h(x)\phi(x) \right\} \tag{A.10}$$

$$\frac{\partial\phi(x,t)}{\partial t} = -\Gamma\left(\frac{\delta\beta\mathcal{F}[\phi]}{\delta\phi(x)}\right) + \xi(x,t) \tag{A.11}$$

The random driving force, ξ, is Gaussian noise, uncorrelated in time.

$$\langle \xi(x,t) \rangle = 0 \tag{A.12}$$

$$\langle \xi(x,t)\xi(x',t') \rangle = L(x-x')\delta(t-t') \tag{A.13}$$

To compute the Einstein relation for this theory we start by calculating the pair correlation function using the equilibrium partition function and Boltzmann statistics.

A.2.1 The partition function route

In equilibrium the probability of particular field configuration is given by the Boltzmann distribution.

$$\mathcal{P}_{eq}[\phi] = \frac{e^{-\beta \mathcal{F}[\phi]}}{\mathcal{Z}[h(x)]} \tag{A.14}$$

Where, $\mathcal{Z}[h(x)]$ is the partition functional and is given by a path integral over all field configurations.

$$\mathcal{Z}[h(x)] = \int \mathcal{D}[\phi] e^{-\beta \mathcal{F}[\phi]} \tag{A.15}$$

Evaluation of the partition function is of some importance because it plays the role of a moment generating function.

$$\frac{1}{\mathcal{Z}[h]} \frac{\delta^n \mathcal{Z}[h]}{\delta h(x_1) ... \delta h(x_n)} = \langle \phi(x_1) ... \phi(x_n) \rangle \tag{A.16}$$

In general the partition function cannot be computed directly, but in the special case of Gaussian free energies it can. To that end we consider expanding ϕ around an equilibrium solution, $\phi(x) = \phi_0 + \Delta\phi(x)$, and keeping terms to quadratic order in the free energy.

$$\beta \mathcal{F}[\Delta\phi] = \int dr \left\{ \frac{1}{2} \Delta\phi(x) \left(r - \nabla^2 + \frac{u}{2}\phi_0^2 \right) \Delta\phi(x) - h(x)\Delta\phi(x) \right\} \tag{A.17}$$

Here the partition function is written in a suggestive form. As stated previously, functional integrals are difficult to compute in general, but Gaussian functional integrals do have a solution.

Computing the Pair correlation function in the Gaussian approximation

To compute the pair correlation function we use the Fourier space variant of the partition function,

$$\mathcal{Z}[\tilde{h}(k)] \propto \exp\left\{\frac{1}{2}\int dk\, \frac{h(k)h^*(k)}{r+\frac{u}{2}\phi_0^2+|k|^2}\right\}. \tag{A.18}$$

The pair correlation function, $\langle\Delta\tilde{\phi}(k)\Delta\tilde{\phi}^*(k)\rangle$, is then computed using equation A.16.

$$\left\langle\Delta\tilde{\phi}(k)\Delta\tilde{\phi}^*(k')\right\rangle = \frac{2\pi\delta(k+k')}{r+\frac{u}{2}\phi_0^2+|k|^2} \tag{A.19}$$

A.2.2 The Equation of Motion Route

The equation of motion supplies a second method for evaluating the pair correlation function in equilibrium.

$$\frac{\partial\phi}{\partial t} = -\Gamma\left((r-\nabla^2)\phi(x,t)+\frac{u}{3!}\phi^3(x,t)\right)+\xi(x,t), \tag{A.20}$$

Our equation of motion, can be linearized around an equilibrium solution, ϕ_0, just as we did in the partition function route to the pair correlation function. In a similar vain, we will Fourier transform the equation of motion as well.

$$\frac{\partial\Delta\tilde{\phi}(k,t)}{\partial t} = -\Gamma\left((r+\frac{u}{2}\phi_0+|k|^2)\Delta\tilde{\phi}(k,t)\right)+\xi(x,t) \tag{A.21}$$

Comparing with our generalized approach we can read of $M(k,k')$ from the lineared equation of motion:

$$M(k,k') = -\Gamma\left((r+\frac{u}{2}\phi_0+|k|^2)\right)\delta(k+k') \tag{A.22}$$

Finally, once we compute the generalized Einstein relation with our specific pair correlation and $M(k,k')$ we find,

$$L(k,k') = 2\Gamma\delta(k+k'), \tag{A.23}$$

Or equivalently,

$$L(x,x') = 2\Gamma\delta(x-x'). \tag{A.24}$$

A.3 Example 2 - Time Dependent Density Functional Theory

In time dependent density functional theory (TDDFT) we have an equation of motion of the following form,

$$\frac{\partial\rho(r,t)}{\partial t} = D_0\nabla\cdot\left[\rho(r,t)\nabla\left(\frac{\delta\mathcal{F}[\rho]}{\delta\rho}\right)\right] + \xi(r,t) \tag{A.25}$$

Where, D_0 is the equilibrium diffusion constant and ξ is the stochastic driving force. We assume once again that the driving force has no bias, but we now allow the noise strength to be a generic kernel $L(r,r')$.

$$\langle\xi(r,t)\rangle = 0 \tag{A.26}$$

$$\langle\xi(r,t)\xi(r',t')\rangle = L(r,r')\delta(t-t') \tag{A.27}$$

A.3.1 Pair Correlation from the Partition Functional

Just like with the phi^4 model we want to expand our free energy functional around an equilibrium solution. In this case our free energy functional is generic so this expansion is

purely formal.

$$\mathcal{F}[\rho] = \mathcal{F}_{eq} + \beta \int dr \left(\frac{\delta \mathcal{F}[\rho]}{\delta \rho(r)} \right) \Bigg|_{\rho_{eq}} \Delta\rho(r) + \frac{1}{2} \int dr \int dr' \Delta\rho(r) \left(\frac{\delta^2 \mathcal{F}[\rho]}{\delta\rho(r)\delta\rho(r')} \right) \Bigg|_{\rho_{eq}} \Delta\rho(r') \tag{A.28}$$

The first term we can neglect as it adds an overall scale to the partition function that will not affect any of moments. Second moment only shifts the average so we can ignore it as well and so we're left with a simple quadratic free energy once again.

$$\mathcal{F}[\rho] = \frac{1}{2} \int dr \int dr' \Delta\rho(r) \Gamma^{-1}(r, r') \Delta\rho(r') \tag{A.29}$$

Where, $\Gamma^{-1}(r, r')$ is the second functional derivative of the free energy functional in equilibrium. Computing the pair correlation function from the partition function yields, as might be expected,

$$\langle \Delta\rho(r) \Delta\rho(r') \rangle = \Gamma(r, r') \tag{A.30}$$

A.3.2 Linearing the equation of motion

Linearizing the equation of motion about an equilibrium solution we find the following form,

$$\frac{\partial \Delta\rho(r,t)}{\partial t} = D_0 \nabla \cdot \left[\rho_{eq}(r) \nabla \left(\Gamma^{-1}(r, r') * \Delta\rho(r', t) \right) \right] + \xi(r, t) \tag{A.31}$$

Once again we can read of the kernel $M(r, r')$ from the linearized equation.

$$M(r, r\prime) = D_0 \nabla \cdot \left[\rho_{eq}(r) \nabla \left(\Gamma^{-1}(r, r') \right) \right] \tag{A.32}$$

Plugging into the generalized Einstein relation, we find a the factors of the pair correlation cancel giving a simple form for the kernel $L(r, r')$.

$$L(r, r') = -2D_0 \nabla \cdot \left(\rho_{eq}(r) \nabla \right) \delta(r - r') \tag{A.33}$$

Appendix B

Gaussian Functional Integrals

Gaussian Functional Integrals

In the study of the statistical physics of fields we often encounter functional integrals of the form,

$$\mathcal{Z}[h(x)] = \int \mathcal{D}[\phi] \exp\left\{ - \int dx \int dx' \left[\frac{1}{2} \phi(x) \mathbf{K}(x, x') \phi(x') \right] + \int dx \left[h(x) \phi(x) \right] \right\}. \quad \text{(B.1)}$$

Solutions to this integral are not only important in there own right but are also the basis perturbative techniques. The detail of how to solve this integral can be found in [20] and are repeated here for the convenience of the reader.

This integral is simply the continuum limit of a multivariable Gaussian integral,

$$\mathcal{Z}[\mathbf{h}] = \int \prod_i dx_i \exp\left\{ -\frac{1}{2} \sum_i \sum_j x_i \, \mathbf{K}_{ij} \, x_j + \sum_i h_i x_i \right\}, \quad \text{(B.2)}$$

For which the solution is,

$$\mathcal{Z}[\mathbf{h}] = \sqrt{\frac{2\pi}{\det(\mathbf{K})}} \exp\left\{ \frac{1}{2} \sum_i \sum_j h_i \mathbf{K}^{-1}_{ij} h_j \right\}. \quad \text{(B.3)}$$

In the continuum limit, the solution has an analogous form.

$$\mathcal{Z}[h(x)] \propto \exp\left\{\int dx \int dx' \left[\frac{1}{2}h(x)\mathbf{K}^{-1}(x,x')h(x')\right]\right\} \tag{B.4}$$

Where $\mathbf{K}^{-1}$ is defined by,

$$\int dx'\mathbf{K}(x,x')\mathbf{K}^{-1}(x',x'') = \delta(x-x''). \tag{B.5}$$

Ultimately, we don't need to worry about the constant of proportionality in equation B.4 because we'll be dividing this contribution when calculating correlation functions.

Appendix C

Binary Correlation Functions

When developing the binary PFC model we often change variables from ρ_A and ρ_B to n and c. This change of variable is helpful in identifying the results of the PFC theory with established results in the field as concentration and total density are more commonly used in the field of material science. Computing the bulk terms (ie., $\Delta\mathcal{F}_{mix}[n,c]$ and $\Delta\mathcal{F}_{id}[n]$ from equation 4.6 and 4.5) is a matter of substitution and simplification but computing the change of variables for excess free energy can be more subtle. When computing the pair correlation terms, careful application of our assumption that c varies over a much longer length scale than n must be applied to get the correct solution. The goal, ultimately, is to find C_{nn}, C_{nc}, C_{cn} and C_{cc} in the following expression,

[Stopped reviewing here! continue hhere in future]

$$\Delta\rho_A\,\rho_0 C_{AA} * \Delta\rho_A + \Delta\rho_A\,\rho_0 C_{AB} * \Delta\rho_B + \Delta\rho_B\,\rho_0 C_{BA} * \Delta\rho_A + \Delta\rho_B\,\rho_0 C_{BB} * \Delta\rho_B = \quad \text{(C.1)}$$
$$(n\,C_{nn} * n + n\,C_{nc} * \Delta c + \Delta c\,C_{cn} * n + \Delta c\,C_{cc} * \Delta c)\,.$$

We begin by rewriting $\Delta\rho_B$,

$$\begin{aligned}\Delta\rho_B &= \rho c - \rho_0 c_0 \\ &= \rho c - \rho c_0 + \rho c_0 - \rho_0 c_0 \\ &= \Delta\rho c + \rho_0 \Delta c,\end{aligned}$$

Followed by rewriting $\Delta\rho_A$,

$$\begin{aligned}\Delta\rho_A &= \rho(1-c) - \rho_0(1-c_0) \\ &= \Delta\rho(1-c) - \rho_0\Delta c.\end{aligned}$$

With those forms established, we can expand $\Delta\rho_B\, C_{BB} * \Delta\rho_B$:

$$\begin{aligned}\Delta\rho_B C_{BB} * \Delta\rho_B &= (\Delta\rho c + \rho_0\Delta c)\, C_{BB} * (\Delta\rho c + \rho_0\Delta c) \\ &= \Delta\rho c\, C_{BB} * (\Delta\rho c) \\ &+ \rho_0\Delta c\, C_{BB} * (\Delta\rho c) \\ &+ \rho_0\, (\Delta\rho c)\; C_{BB} * \Delta c \\ &+ \rho_0^2\Delta c\, C_{BB} * \Delta c.\end{aligned} \tag{C.2}$$

If we examine one term in this expansion in detail, we note that we can simplify by using the long wavelength approximation for the concentration field,

$$\begin{aligned}\Delta\rho c\, C_{BB} * \Delta\rho c &= \Delta\rho(r)c(r) \int dr' C_{BB}(r-r')\Delta\rho(r')c(r') \\ &\approx \Delta\rho(r)c^2(r) \int dr' C_{BB}(r-r')\Delta\rho(r').\end{aligned} \tag{C.3}$$

This is because the concentration field can be considered ostensibly constant over the length scale in which $C_{BB}(r)$ varies. Recall that the pair correlation function typically decays to

zero on the order of several particle radii. Using this approximation we can rewrite equation C.2 as,

$$\begin{aligned}\Delta\rho_B\, C_{BB} * \Delta\rho_B = {} & \Delta\rho \left(c^2\, C_{BB}\right) * \Delta\rho \\ & + \rho_0 \Delta c \left(c\, C_{BB}\right) * \Delta\rho c \\ & + \rho_0 \Delta\rho \left(c\, C_{BB}\right) * \Delta c \\ & + \rho_0^2 \Delta c\, C_{BB} * \Delta c.\end{aligned} \tag{C.4}$$

Repeating this procedure with the remaining three terms and then regrouping we can easily identify the required pair correlations.[1]

$$C_{nn} = \rho_0 \left(c^2\, C_{BB} + (1-c)^2\, C_{AA} + 2c(1-c)\, C_{AB}\right) \tag{C.5}$$

$$C_{nc} = C_{cn} = \rho_0 \left(c\, C_{BB} - (1-c)\, C_{AA} + (1-2c)\, C_{AB}\right) \tag{C.6}$$

$$C_{cc} = \rho_0 \left(C_{BB} + C_{AA} - 2C_{AB}\right) \tag{C.7}$$

[1]Note that we may also take advantage of the fact that $C_{AB} = C_{BA}$.

Appendix D

Algorithms

Presented here is a general approach to integrating nonlinear stochastic partial differential equations. An integration scheme for the binary XPFC equations of motion is presented as an application.

D.1 Semi-Implicit Spectral Methods for Systems of First Order PDEs

To start, we consider the general case of time stepping a system of non-linear first-order PDE's. Specifically, we are going to look at a set of stochastic non-linear PDE's,

$$\frac{\partial \overline{\psi}(x,t)}{\partial t} = \mathcal{G}\left[\overline{\psi}(x,t)\right] + \overline{\xi}(x,t), \tag{D.1}$$

Where,

$\overline{\psi}(x,t)$ is a vector of our fields of interest (ex: (n, c)) and we've used $\bar{\cdot}$ to denote a vector,

$\mathcal{G}$ is some driving force for our fields and,

$\overline{\xi}(x,t)$ is the stochastic driving force with variances given by a generalized Einstein relationship.

To develop a semi-implicit method we start by splitting the functional $\mathcal{G}$ into linear and non-linear components,

$$\frac{\partial\overline{\psi}(x,t)}{\partial t} = \overline{\overline{\mathcal{L}}}(x,x') * \overline{\psi}(x',t) + \mathcal{NL}\left[\overline{\psi}\right] + \overline{\xi}(x,t) \tag{D.2}$$

Where,

$\overline{\overline{\mathcal{L}}}$ denotes the linear contribution and $\overline{\overline{\cdot}}$ denotes a matrix,

$*$ matrix multiplication and integration over the repeated variable and,

$\mathcal{NL}$ is the non-linear component of the the functional $\mathcal{G}$.

In a special set of PDE's the kernel $\overline{\overline{\mathcal{L}}}$ is translationally invariant. When this is the case, the convolution theorem can be used to write the linear functional as an algebraic product in Fourier space.

$$\frac{\partial\overline{\psi}(k,t)}{\partial t} = \overline{\overline{\mathcal{L}}}(k)\overline{\psi}(k,t) + \mathcal{F}\left[\mathcal{NL}\left[\overline{\psi}\right]\right] + \overline{\xi}(k,t) \tag{D.3}$$

Where, $\mathcal{F}[\,\cdot\,]$ denotes a Fourier transform. We now consider our fields on a discrete grid with Δk spacing between Fourier modes and Δt spacing between times such that we might define,

$$\overline{\psi}_j^n \equiv \overline{\psi}(j\Delta k, n\Delta t). \tag{D.4}$$

To develop a generic approach to time stepping we consider evaluating our field between grid points in time (eg. at $\overline{\psi}_j^{n+\gamma}$ where $\gamma \in [0,1]$).

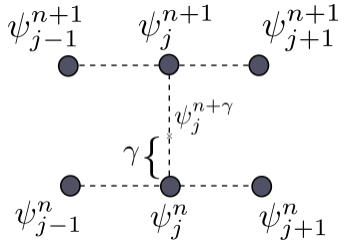

Figure D.1: Schematic of time step

To first order we can approximate this value as a linear interpolation of the value at n and the value at $n+1$.

$$\overline{\psi}_j^{n+\gamma} = (1-\gamma)\overline{\psi}_j^n + \gamma\overline{\psi}_j^{n+1} \tag{D.5}$$

We can also approximate the time derivative $\partial_t\overline{\psi}$ as,

$$\frac{\partial\overline{\psi}}{\partial t} = \frac{\overline{\psi}_j^{n+1} - \overline{\psi}_j^n}{\Delta t} + \frac{1-2\gamma}{2}\frac{\partial^2\overline{\psi}}{\partial t^2}\Delta t + ... \tag{D.6}$$

Deriving different integration schemes is done by evaluating the equation of motion for various values of γ. For example, to recover simple Euler stepping we can evaluate the equation of motion with $\gamma = 0$. The semi-implicit scheme relays on evaluating the non-linear component of the equation of motion at $\gamma = 0$ while the rest of the equation is evaluated at $\gamma = 1$. In this treatment we will evaluate the non-linear component at $\gamma = 0$ but we will leave the rest of the equation unevaluated so that γ can be choosen freely at the end. Substituting these results into equation of motion we find the following result,

$$\frac{\overline{\psi}_j^{n+1} - \overline{\psi}_j^n}{\Delta t} + \frac{1-2\gamma}{2}\frac{\partial^2\overline{\psi}}{\partial t^2}\Delta t = \overline{\overline{\mathcal{L}}}\left((1-\gamma)\overline{\psi}_j^n + \gamma\overline{\psi}_j^{n+1}\right) + \mathcal{F}\left[\mathcal{N}\mathcal{L}\left[\overline{\psi}_j^n\right]\right] + \overline{\xi}_j^{n+\gamma} \tag{D.7}$$

Separating $t = n+1$ terms on the left and $t = n$ terms on the right,

$$\left(\mathbb{1} - \Delta t\gamma\overline{\overline{\mathcal{L}}}\right)\overline{\psi}_j^{n+1} = \left(\mathbb{1} + \Delta t(1-\gamma)\overline{\overline{\mathcal{L}}}\right)\overline{\psi}_j^n + \Delta t\mathcal{F}\left[\mathcal{N}\mathcal{L}\left[\overline{\psi}_j^n\right]\right] + \Delta t\overline{\xi}_j^{n+\gamma} - \frac{1-2\gamma}{2}\frac{\partial^2\overline{\psi}}{\partial t^2}\Delta t^2 \tag{D.8}$$

Finally, we can isolate $\overline{\psi}_j^{n+1}$ by left multiplying by $\left(\mathbb{1} - \gamma\Delta t\overline{\overline{\mathcal{L}}}\right)^{-1}$,

$$\overline{\psi}_j^{n+1} = \left(\mathbb{1} - \Delta t\gamma\overline{\overline{\mathcal{L}}}\right)^{-1}\left(\left(\mathbb{1} + \Delta t(1-\gamma)\overline{\overline{\mathcal{L}}}\right)\overline{\psi}_j^n + \Delta t\mathcal{F}\left[\mathcal{N}\mathcal{L}\left[\overline{\psi}_j^n\right]\right] + \Delta t\overline{\xi}_j^{n+\gamma} - \frac{1-2\gamma}{2}\frac{\partial^2\overline{\psi}}{\partial t^2}\Delta t^2\right) \tag{D.9}$$

The final term on the right hand side emphasizes that if we choose $\gamma = 1/2$ we will have a algorithm that is accurate to second order in time (this is a kind of Crank-Nicolson method). If we choose $\gamma = 1$ we recover a semi-implicit method.

D.2 Applications to the Binary XPFC Model

The binary XPFC model is a good example of a system of first order PDE's like those discussed in the previous discussion. The equations of motion in real space are,

$$\frac{\partial c(x,t)}{\partial t} = M_c \nabla^2 \left((\omega\epsilon - W_c \nabla^2) c + \omega(1+n) \frac{\partial \Delta F_{mix}(c)}{\partial c} - \frac{1}{2} n \left(\frac{\partial C_{eff}}{\partial c} * n \right) \right) + \xi_c(x,t) \tag{D.10}$$

$$\frac{\partial n(x,t)}{\partial t} = M_n \nabla^2 \left((1 - C_{eff}*)\, n - \frac{\eta}{2} n^2 + \frac{\chi}{3} n^3 + \omega \Delta F_{mix} \right) + \xi_n(x,t) \tag{D.11}$$

Where,

ΔF_{mix} is the ideal free energy of mixing $c \log\left(\frac{c}{c_0}\right) + (1-c)\log\left(\frac{1-c}{1-c_0}\right)$

With reference to the formalism we've already established our task is now to seperate out the linear and non-linear components of these equations of motion. To do this, we expand the concentration and density around constant references c_* and n_*. Doing so leads to an expression of $\overline{\overline{\mathcal{L}}}$,

$$\overline{\overline{\mathcal{L}}} = \begin{bmatrix} -M_c k^2 \left(\omega \left(\epsilon - \frac{1}{c_*^2 - c_*} \right) + W_c k^2 \right) & -M_c k^2 \omega \log\left(\frac{(c_0-1)c_*}{c_0(c_*-1)} \right) \\ -M_n k^2 \omega \log\left(\frac{(c_0-1)c_*}{c_0(c_*-1)} \right) & -M_n k^2 \left(1 - C_{eff}|_{c_*}(k) \right) \end{bmatrix} \tag{D.12}$$

Important to note in the structure of $\overline{\overline{\mathcal{L}}}$ is that it is diagonal in the limit of small ω. In the approximation that it is diagonal, previous algorithms for the binary XPFC model are recovered where, to linear order, concentration and density may be independently integrated. Another interesting case is that of $M_n = M_c$ where the matrix is symmetric and thus has orthogonal eigenvectors. We proceed by considering this simplified case where the concentration and density are weakly coupled at the linear order and may be integrated seperately.

D.2.1 Algorithm for the Concentration $c(x,t)$

The concentration equation of motion is,

$$\partial_t \tilde{c} = -M_c k^2 \left(\omega\epsilon\tilde{c} + W_c k^2 \tilde{c} + \mathcal{F}\{NL(c)\}\right) + \tilde{\xi}. \tag{D.13}$$

Where $NL(c)$ is the non-linear term and ξ is the drive noise.

$$NL(c) = \omega(1+n)\left(\ln\left(\frac{c}{c_0}\right) - \ln\left(\frac{1-c}{1-c_0}\right)\right) - \frac{1}{2}n\left(C^n_{eff} * n\right) \tag{D.14}$$

Now if we think about the solution to this equation at time $t^{n+\xi}$ time between t^n and t^{n+1} we express the solution as an interpolation between the solutions at the earlier and later times.

$$\tilde{c}^{n+\xi}_k = (1-\xi)\tilde{c}^n_k + \xi\tilde{c}^{n+1}_k \tag{D.15}$$

We also find that we can express the time derivative as finite difference plus a correction term.

$$\partial_t \tilde{c} = \frac{\tilde{c}^{n+1}_k - \tilde{c}^n_k}{\Delta t} + \frac{1-2\xi}{2}\frac{\partial^2 \tilde{c}}{\partial t^2}\Delta t + ... \tag{D.16}$$

Using each of these ideas we can rewrite the equation of motion completely, with the exception of the nonlinear term, which we evaluate a the time t^n in keeping with many of the semi-implicit methods published.

$$\frac{\tilde{c}^{n+1}_k - \tilde{c}^n_k}{\Delta t} + \frac{1-2\xi}{2}\frac{\partial^2 \tilde{c}}{\partial t^2}\Delta t = \Lambda(k)\left[(1-\xi)\tilde{c}^n_k + \xi\tilde{c}^{n+1}_k\right] - M_c k^2 \mathcal{F}\{NL(c^n)\} + \tilde{\xi}^n_k \tag{D.17}$$

where,

$$\Lambda(k) = -M_c k^2\left(\omega\epsilon + W_c k^2\right). \tag{D.18}$$

Moving future times to the left and past times to the right we find,

$$\tilde{c}_k^{n+1} = \hat{P}\tilde{c}_k^n + \hat{Q}\mathcal{F}\{NL(c^n)\}_k + \hat{L}\tilde{\xi}_k^n + \frac{2\xi - 1}{2}\frac{\partial^2 \tilde{c}}{\partial t^2}\Delta t^2 \tag{D.19}$$

Where the operators $\hat{P}$, $\hat{Q}$ and $\hat{L}$ are,

$$\hat{P} = 1 + \frac{\Delta t \Lambda(k)}{1 - \xi \Delta t \Lambda(k)} \tag{D.20}$$

$$\hat{Q} = -\frac{M_c k^2 \Delta t}{1 - \Delta t \xi \Lambda(k)} \tag{D.21}$$

$$\hat{L} = \frac{\Delta t}{1 - \Delta t \xi \Lambda(k)} \tag{D.22}$$

Different values of ξ lead to different integration schemes. The $\xi = 0$ corresponds to euler time stepping in fourier space, while $\xi = 1$ yields the often used semi-implicit fourier method. There is an import case in which we choose $\xi = 1/2$ where the algorithm becomes accurate to second order in time. This is the Crank-Nicholson fourier method.

D.2.2 Algorithm for the Total Density $n(x,t)$

We can develop an algorithm for the equation of motion fo the total density in the same way that we did with concentration. The equation of motion for the total density in fourier space looks like,

$$\partial_t \tilde{n}(k,t) = -M_n k^2 \left(\tilde{n} + \mathcal{F}\{NL(n)\}\right) + \tilde{\xi} \tag{D.23}$$

Where now the nonlinear term is,

$$NL(n) = -\eta\frac{n^2}{2} + \chi\frac{n^3}{3} + \Delta f_{mix}(c) - C_{eff}^n * n \tag{D.24}$$

Note that the convolution term is nonlinear because of an implicit dependance on the concentration. Now, in principle, you could compute that pair correlation function every time

step for a more accurate linear propagator, but here we will not consider that.

Here again, we find the same structure as previously:

$$\tilde{n}_k^{n+1} = \hat{P}\tilde{n}_k^n + \hat{Q}\mathcal{F}\{NL(n^n)\}_k + \hat{L}\tilde{\xi}_k \tag{D.25}$$

Here, the operators $\hat{P}$, $\hat{Q}$ and $\hat{L}$ are:

$$\hat{P} = 1 - \frac{\Delta t M_n k^2}{1 + \xi \Delta t M_n k^2} \tag{D.26}$$

$$\hat{Q} = -\frac{M_c k^2 \Delta t}{1 + \Delta t \xi M_n k^2} \tag{D.27}$$

$$\hat{L} = \frac{\Delta t}{1 + \Delta t \xi M_n k^2} \tag{D.28}$$

Bibliography

[1] Eli Alster, K. R. Elder, Jeffrey J. Hoyt, and Peter W. Voorhees. Phase-field-crystal model for ordered crystals. *Phys. Rev. E*, 95:022105, Feb 2017.

[2] Andrew J Archer and Markus Rauscher. Dynamical density functional theory for interacting brownian particles: stochastic or deterministic? *Journal of Physics A: Mathematical and General*, 37(40):9325, 2004.

[3] K R Elder and Z-F Huang. A phase field crystal study of epitaxial island formation on nanomembranes. *Journal of Physics: Condensed Matter*, 22(36):364103, 2010.

[4] K. R. Elder, Nikolas Provatas, Joel Berry, Peter Stefanovic, and Martin Grant. Phase-field crystal modeling and classical density functional theory of freezing. *Phys. Rev. B*, 75:064107, Feb 2007.

[5] K.R. Elder, K. Thornton, and J.J. Hoyt. The kirkendall effect in the phase field crystal model. *Philosophical Magazine*, 91(1):151–164, 2011.

[6] Pep Español and Hartmut Löwen. Derivation of dynamical density functional theory using the projection operator technique. *The Journal of Chemical Physics*, 131(24):244101, 2009.

[7] Vahid Fallah, Andreas Korinek, Nana Ofori-Opoku, Nikolas Provatas, and Shahrzad Esmaeili. Atomistic investigation of clustering phenomenon in the al–cu system: Three-

dimensional phase-field crystal simulation and hrtem/hrstem characterization. *Acta Materialia*, 61(17):6372 – 6386, 2013.

[8] Vahid Fallah, Nana Ofori-Opoku, Jonathan Stolle, Nikolas Provatas, and Shahrzad Esmaeili. Simulation of early-stage clustering in ternary metal alloys using the phase-field crystal method. *Acta Materialia*, 61(10):3653 – 3666, 2013.

[9] Vahid Fallah, Jonathan Stolle, Nana Ofori-Opoku, Shahrzad Esmaeili, and Nikolas Provatas. Phase-field crystal modeling of early stage clustering and precipitation in metal alloys. *Phys. Rev. B*, 86:134112, Oct 2012.

[10] Ronald Forrest Fox and George E. Uhlenbeck. Contributions to non-equilibrium thermodynamics. i. theory of hydrodynamical fluctuations. *Physics of Fluids*, 13(8):1893–1902, 1970.

[11] Nirmalendu Ganai, Arnab Saha, and Surajit Sengupta. Colloidal particles in a drying suspension: A phase field crystal approach. *European Physical Journal E – Soft Matter*, 36(8):1 – 10, 2013.

[12] J. Willard Gibbs. *Elementary principles in statistical mechanics*. 1960.

[13] Michael Greenwood, Nana Ofori-Opoku, Jörg Rottler, and Nikolas Provatas. Modeling structural transformations in binary alloys with phase field crystals. *Phys. Rev. B*, 84:064104, Aug 2011.

[14] Michael Greenwood, Jörg Rottler, and Nikolas Provatas. Phase-field-crystal methodology for modeling of structural transformations. *Phys. Rev. E*, 83:031601, Mar 2011.

[15] Michael Greenwood, Chad Sinclair, and Matthias Militzer. Phase field crystal model of solute drag. *Acta Materialia*, 60(16):5752 – 5761, 2012.

[16] Jean-Pierre Hansen and Ian R. McDonald. Appendix b: Two theorems in density functional theory. In Jean-Pierre Hansen and Ian R. McDonald, editors, *Theory of*

Simple Liquids (Fourth Edition), pages 587 – 589. Academic Press, Oxford, fourth edition edition, 2013.

[17] Jean-Pierre Hansen and Ian R. McDonald. Chapter 6 - inhomogeneous fluids. In Jean-Pierre Hansen and Ian R. McDonald, editors, *Theory of Simple Liquids (Fourth Edition)*, pages 203 – 264. Academic Press, Oxford, fourth edition edition, 2013.

[18] Jean-Pierre Hansen and Loup Verlet. Phase transitions of the lennard-jones system. *Phys. Rev.*, 184:151–161, Aug 1969.

[19] E. T. Jaynes. Information theory and statistical mechanics. *Phys. Rev.*, 106:620–630, May 1957.

[20] M. Kardar. *Statistical Physics of Fields*. June 2006.

[21] John G. Kirkwood. Quantum statistics of almost classical assemblies. *Phys. Rev.*, 44:31–37, Jul 1933.

[22] John G. Kirkwood and Elizabeth Monroe. Statistical mechanics of fusion. *The Journal of Chemical Physics*, 9(7):514–526, 1941.

[23] Ryogo Kubo. Generalized cumulant expansion method. *Journal of the Physical Society of Japan*, 17(7):1100–1120, 1962.

[24] L.D. LANDAU and E.M. LIFSHITZ. Chapter iii - the gibbs distribution. In L.D. LANDAU and E.M. LIFSHITZ, editors, *Statistical Physics (Third Edition, Revised and Enlarged)*, pages 79 – 110. Butterworth-Heinemann, Oxford, third edition, revised and enlarged edition, 1980.

[25] Melvin Lax. Fluctuations from the nonequilibrium steady state. *Rev. Mod. Phys.*, 32:25–64, Jan 1960.

[26] Guang-Ming Lu, Yan-Li Lu, Ting-Ting Hu, and Zheng Chen. Phase field crystal study on the phase boundary migration induced by the kirkendall effect. *Computational Materials Science*, 106:170 – 174, 2015.

[27] Yanli Lu, Yingying Peng, and Zheng Chen. A binary phase field crystal study for liquid phase heteroepitaxial growth. *Superlattices and Microstructures*, 97:132 – 139, 2016.

[28] Umberto Marini Bettolo Marconi and Pedro Tarazona. Dynamic density functional theory of fluids. *Journal of Physics: Condensed Matter*, 12(8A):A413, 2000.

[29] Joseph E. Mayer and Elliott Montroll. Molecular distribution. *The Journal of Chemical Physics*, 9(1):2–16, 1941.

[30] Heather A. Murdoch and Christopher A. Schuh. Stability of binary nanocrystalline alloys against grain growth and phase separation. *Acta Materialia*, 61(6):2121 – 2132, 2013.

[31] L. Onsager and S. Machlup. Fluctuations and irreversible processes. *Phys. Rev.*, 91:1505–1512, Sep 1953.

[32] T. V. Ramakrishnan and M. Yussouff. First-principles order-parameter theory of freezing. *Phys. Rev. B*, 19:2775–2794, Mar 1979.

[33] David Ronis, Itamar Procaccia, and Jonathan Machta. Statistical mechanics of stationary states. vi. hydrodynamic fluctuation theory far from equilibrium. *Phys. Rev. A*, 22:714–724, Aug 1980.

[34] George E. Uhlenbeck and Erich Beth. The quantum theory of the non-ideal gas i. deviations from the classical theory. *Physica*, 3(8):729 – 745, 1936.

[35] E. Wigner. On the quantum correction for thermodynamic equilibrium. *Phys. Rev.*, 40:749–759, Jun 1932.